Fast MHD Dissipative Processes

Fausto T. Gratton, Laurence Bender and Graciela Gnavi

Instituto de Física del Plasma, Consejo Nacional de Investigaciones Cientificas y Técnicas and Facultad de Ciencias Exactas y Naturales

Departamento de Física, Universidad de Buenos Aires

Ciudad Universitaria, Pab.I, 1428 Buenos Aires, Argentina

Received November 13, 1995

We study the time evolution of current sheets under the influence of stagnation point flows driven by external forces. It is shown that significant physical processes occur during the formation of the current sheet, which is originated from the advection of a sparse magnetic flux. The advection and intensification of the magnetic field at a stagnation flow can give rise to large amounts of Joule dissipation over hydrodynamic time scales. Depending on the balance between the incoming magnetic flux and the dissipation rate, these effects may lead to an accelerated extinction of the magnetic field, the formation of steady state dissipative layers, or to solutions that grow without bound linearly with time. The basic elements of the flow enhanced dissipation mechanism are discussed using order of magnitude considerations. Analytic time dependent solutions that describe the evolution of the magnetic field are obtained for planar flows. Starting from generic initial and boundary conditions for the magnetic field component lying on the plane of the flow, it is shown that the sublayer in which a change of sign of the magnetic field occurs tends to vanish in a short time during the formation of the current sheet. On the other hand, the magnetic field component normal to the flow plane is always rapidly extinguished. Thus, configurations commonly considered as models to steady state reconnection or tearing instability studies, are exceptional cases rather than generic magnetic structures. In three dimensional stagnation flows, all magnetic fields not sustained by a continuous injection of magnetic energy are completely annihilated in a few hydrodynamic times. Self similar solutions that describe the amplification and decay of the magnetic field for planar and axial-symmetric flows are also obtained. Several applications, including solar plasma current sheaths, the dayside magnetospheric stagnation point, and the formation of hot spots in the Plasma Focus experiments, are discussed. The theory of the stability of these dissipative structures is commented upon. Thermal effects due to the rise of the temperature in the current sheath and the ensuing conductivity increment, enhance the amplification and extintion processes. These effects are illustrated with numerical solution examples. Finally, compressibility effects that set a limit to the validity of the solutions are briefly outlined.

I. Introduction

The material presented here (prepared for the VI Latin American Workshop on Plasma Physics, Foz do Iguaçu, 24–28 October, 1994) is based on research work performed at the Instituto de Física del Plasma (CONICET and FCEyN/UBA), Buenos Aires. A more precise title should be "fast MHD dissipative processes associated with stagnation point flows." The content is mainly about convection and stretching of magnetic field lines in this kind of flows. Convection carries the magnetic lines toward the current layer and concentrates the magnetic field. Convection also intensifies the cooling of the current sheath by transporting cold material from external regions. The stretching of magnetic field lines increases the magnetic field intensity at the expense of the work done by the pressure in the flow. The amplification of the magnetic field increases the Joule dissipation. These effects may lead to an accelerated extinction of the field, or to a steady state with strongly dissipative layers, depending on the balance between the incoming magnetic flux and the

dissipation rate.

Current sheets are characteristic regions in laboratory and astrophysical plasmas, where magnetic energy is concentrated. These are scenarios for the fast release of the stored energy into other forms of energy by reconnection of magnetic lines, Joule heating, or resistive instabilities.[3,40,59] By a fast process we mean a magnetic evolution, amplification or extinction, faster than the ordinary diffusion time $\tau_D \sim L^2/\nu_m$ (L: scale length of the field; ν_m: magnetic diffusivity) or diffusion speed $v_D \sim \nu_m/L$. The tearing instability of a current sheath in diffusive equilibrium[14,59,58] has a growth rate $\gamma \sim (\tau_D \tau_A)^{-1/2}$ ($\tau_A = L/V_A$; V_A: Alfvén speed), so that $\tau_A << \tau = \gamma^{-1} << \tau_D$. This is a process faster than diffusion but slower than the Alfven time. The reconnection of magnetic lines[1,3,42,49,57,59] may occur with the so called Sweet-Parker scaling,[37,54] that leads to the reconnection speed (v_i: influx speed) $v_i/V_{Ai} \sim 1/S_i^{1/2}$ ($V_{Ai} = B_i/\sqrt{4\pi\rho}$, Alfven speed at inflow magnetic field; $S_i = V_{Ai}L/\nu_m$, Lundquist number at inflow values). This speed is to be compared with $v_D/V_{Ai} \sim 1/S_i$, so that it is much larger than the diffusion speed. The corresponding time scale $\tau_{SP} = L/v_i \sim \tau_D/S_i^{1/2}$ is much shorter than τ_D for $S_i >> 1$, but it is still too long for reconnection precesses conjectured to happen, e.g., in solar physics. The Petsheck reconnection model[39,49,57] allows much larger values $v_i/V_{Ai} \sim \pi/8lnS_i$ and can be considered as a very fast process. However, it has been questioned during the last decade as incompatible with numerical solutions of the MHD dissipative equations, originating a lively pro and con debate about its validity. [2,1,3,12,25,40,41,42]

The current sheath build-up or extinction processes studied in these lectures (no reconnection considered) are driven by external forces, and the Alfvenic Mach number $M_A = v_i/V_{Ai}$ can, in principle, be arbitrarily large (see Section IX). The characteristic time scale, being of the order of the hydrodynamic time, is much shorter than the Sweet-Parker scaling or the tearing instability growth time. The large dissipation rate may produce a rise of the temperature in the current sheath and a conductivity increment. The magnetic field grows further and the current layer shrinks, with an additional rise of the Joule dissipation. The field amplification may become so large as to exhaust the strength of the external driver, or produce a substantial density variation (plasma depletion) which, however, is not accounted for in the analysis reported here.

The time evolution of resistive layers under the influence of a stagnation flow has not been sufficiently explored yet, as can be noted in surveys of the field (e. g., [1,40,49,57]). We show here that advection and intensification of magnetic fields (by line 'stretching') at a stagnation flow, as can develop when the plasma is locally squeezed by external agents, may produce considerable amount of Joule dissipation in a short time. This mechanism can provide explanations for fast dissipation rates in several plasma systems, often rendering 'anomalous' resistivity hypotheses superfluous. Our purpose is to point out the significant physical consequences of the transient processes that occur during the formation of a current sheet, originated from the advection of a sparse magnetic seed or from external continuous injection of magnetic flux.

It is shown that advection and enhancement of a magnetic field in a stagnation flow may produce in a short time t_e a large Joule dissipation (D per unit area and per unit time) in a small slab (width δ). The scaling is (approximately) $t_e/t_h = (1/2)\ln R_m, D = Wo\sqrt{R_m}/t_h, \delta/h_o = 1/\sqrt{R_m}$. Here $t_h = h_o/U_o$ is the hydrodynamic time (h_o, U_o, characteristic length and speed, respectively), R_m is the magnetic Reynolds number assumed to be large, and W_o is the magnetic energy (per unit area) contained in a slab of width h_o at $t = 0$.[17] A set of analytic time dependent solutions describe the evolution of current sheets at a plasma stagnation flow, where considerable intensification of magnetic energy and high dissipation rates occur. In planar geometry it is shown that (without flux injection) a generic magnetic field component, lying on the plane of the flow, after a transient where amplification and decay of its odd part takes place, leaves a large even remnant concentrated in a thin resistive slab. If the external cause of the plasma inflow is switched off, the magnetic layer extinguishes at a much slower rate than the corresponding build-up process. When a continuous injection of magnetic flux takes place it is found that in general the even component of the magnetic field becomes dominant over the odd part, after some time. The exception is the special case where the incoming magnetic flux from both sides is carefully bal-

anced. Thus, starting from generic initial and boundary conditions, one may expect that the sublayer in which a change of sign of the magnetic field occurs, vanishes in a short time during the current sheet formation. As a consequence, possible steady state scenarios envisaged for reconnection processes or tearing instabilities, may not materialize.[18] On the other hand, a magnetic field component normal to the flow plane is always extinguished, even with constant flux injection. There is no amplification effect for this component, except in systems driven by injected flux growing in time. Stagnation flows in three dimensions (axially symmetric diverging outflows) have magnetic field evolution properties quite different from those described by the planar current sheath models. The magnetic field is amplified in a first stage, but is ultimately extinguished when there is no flux injection. Steady state current sheaths that are weaker than in the planar case can be sustained only by flux injection which grows in time.

A radial convergence of a plasma flow with outlets along the axis (in cylindrical geometry) is driven by an azimuthal magnetic field component. It is shown that a magnetic field component parallel to the axis of the plasma configuration is amplified evolving into a strongly dissipative filament in very short times. The results may explain the formation of hot spots in the plasma column stage of Plasma Focus experiments.[15] Consequences of the current sheath models for solar plasma current sheaths, and the dayside magnetospheric stagnation point are also discussed. Thermal effects enhance the amplification and extinction processes, while plasma compressibility sets a limit to the validity of the solutions studied here, and may affect the magnetic field build-up. These topics, still open, are briefly outlined.

Although our subject is related to the fields of reconnection of magnetic field lines, tearing instabilities, or MHD dynamo theories, among others, no attempt has been made to enter in these areas, except for a few short remarks. These are, however, very large and important subjects. The interested readers should familiarize themselves with these related areas, consulting the major surveys cited here. During the preparation of the paper two important monographs,[3,37], have been published. Our work complements the progress achieved by the effort of many authors providing detailed analytical models for some particular processes. These, we believe, are useful to gain further insight in the physics of this complex field.

II. Reduced MHD equations in curvilinear coordinates

II.1 Incompressible flows.

In view of the tutorial nature of these lectures we give here a short review of the basic MHD equations with resistive and viscous diffusion effects and their reduction to a simpler set. This reduction is possible when the system has a manifest translational or rotational symmetry, and the incompressibility condition, $\mathrm{div}\,\mathbf{v} = 0$, allows for the introduction of Euler potential for the flow and magnetic field.

Incompressibility is the natural assumption when dealing with MHD processes in liquids, like those indicated in Table I. In plasmas $\Delta\rho/\rho \sim (1/c_s^2)\Delta p/\rho$, where c_s is the sound speed ($c_s = 9.8 \times 10^5(\gamma T_e/\mu)^{1/2}$ cm s^{-1}; T_e in eV and $\mu = m_i/m_p$). An estimate of $\Delta p/\rho$ in dynamical processes where the plasma speed variation is $\sim U_0$ and the magnetic field may vary $\sim B_0$, is given by $(\Delta p/\rho) \sim U_0^2 + B_0^2/8\pi\rho$, as follows from a comparison of the terms $\mathrm{grad}\,p$, $\mathrm{grad}\,B^2/8\pi$, and $\rho\mathbf{v}.\mathrm{grad}\,\mathbf{v}$ in the equation of motion. Thus, $\Delta p/\rho \sim M^2 + 1/\gamma\beta$, where $M = U/c_s$ is the Mach number and $\beta = 8\pi nKT/B^2 = 4 \times 10^{-11} nT/B^2$ (where T is in eV, n: particles cm^{-3};B is in Gauss). The incompressibility assumption $\Delta\rho/\rho << 1$ is valid if $M^2 << 1$ and $\beta >> 1$ hold during the evolution of the plasma. Note that in this context a static value of β is irrelevant, what counts is the difference of initial and final values, i.e., $\Delta p \sim B\Delta B/4\pi$.

II.2 Basic equations.

When incompressibility and uniform density are assumed, and if the viscous and resistive transport processes in the plasma are isotropic, then the MHD equations can be written as (see, e.g., [1,30,31,40,45]).

$$\begin{aligned}
\operatorname{div}\mathbf{v} &= 0, && (1)\\
-\operatorname{grad}P &= \frac{\partial\mathbf{v}}{\partial t}+\omega\times\mathbf{v}-\frac{1}{c\rho}\mathbf{j}\times\mathbf{B}+\nu\operatorname{curl}\omega, && (2)\\
\frac{1}{\sigma}\mathbf{j} &= \mathbf{E}+\frac{1}{c}\mathbf{v}\times\mathbf{B}-\frac{m_i}{\rho q c}\mathbf{j}\times\mathbf{B}+\operatorname{grad}\left(\frac{m_i}{\rho q}p_e\right), && (3)\\
\frac{4\pi}{c}\mathbf{j} &= \operatorname{curl}\mathbf{B}, && (4)\\
-\frac{1}{c}\frac{\partial\mathbf{B}}{\partial t} &= \operatorname{curl}\mathbf{E}, && (5)\\
\operatorname{div}\mathbf{B} &= 0. && (6)
\end{aligned}$$

In these equations we have used the definitions

$$\omega=\operatorname{curl}\mathbf{v},\qquad P=\frac{p}{\rho}+\frac{1}{2}|\mathbf{v}|^2+V, \tag{7}$$

and the other symbols have the following meanings: $\mathbf{v}$, velocity; $\mathbf{B}$, $\mathbf{E}$, magnetic and electric fields; $\mathbf{j}$, electric current density; p, p_e, plasma and electron pressure; ρ, mass density; ν, σ, kinematical viscosity and electrical conductivity; m_i, q, mass and charge of the plasma ions; V gravitational potential per unit mass. Mechanical cgs units, and electrical ues units are used throughout; c is the speed of light in vacuum. Important restrictions of the set of equations (1)–(6) are:
(i) the plasma density is uniform, $\rho=$ const.,
(ii) ν and σ are assumed to be constants.

Note that Ohm's law, Eq. (3), includes the Hall effect and a thermoelectrical term.

Electrodynamic potentials $\mathbf{A}$, Φ_e, with the gauge choice,

$$\operatorname{div}\mathbf{A}=0 \tag{8}$$

such that

$$\begin{aligned}
\mathbf{B} &= \operatorname{curl}\mathbf{A}, && (9)\\
\mathbf{E} &= -\frac{1}{c}\frac{\partial\mathbf{A}}{\partial t}-\operatorname{grad}\Phi_e, && (10)
\end{aligned}$$

will also be used in the formalism. We now introduce auxilliary variables, all of them with kinematical, i.e., spatio-temporal, dimensions

$$\mathbf{h}\stackrel{def}{=}\frac{\mathbf{B}}{\sqrt{4\pi\rho}},\ \epsilon\stackrel{def}{=}\frac{c\mathbf{E}}{\sqrt{4\pi\rho}},\ \mathbf{a}\stackrel{def}{=}\frac{\mathbf{A}}{\sqrt{4\pi\rho}},\ \phi_e\stackrel{def}{=}\frac{c\Phi_e}{\sqrt{4\pi\rho}},\ \mathbf{J}\stackrel{def}{=}\sqrt{\frac{4\pi}{\rho c^2}}\mathbf{j}, \tag{11}$$

so that we may write, for instance,

$$\frac{1}{c\rho}\mathbf{j}\times\mathbf{B}=\mathbf{J}\times\mathbf{h} \tag{12}$$

for the Lorentz force per unit mass, and

$$\epsilon=-\frac{\partial\mathbf{a}}{\partial t}-\operatorname{grad}\phi_e, \tag{13}$$

instead of Eq. (10). The equations of linear momentum and Ohm's law become

$$\begin{aligned}
-\operatorname{grad}P &= \frac{\partial\mathbf{v}}{\partial t}+\omega\times\mathbf{v}+\nu\operatorname{curl}\omega-\mathbf{J}\times\mathbf{h}, && (14)\\
-\operatorname{grad}Q &= \frac{\partial\mathbf{a}}{\partial t}+\mathbf{h}\times\mathbf{v}+\nu_m\operatorname{curl}\mathbf{h}-\frac{1}{k}\mathbf{J}\times\mathbf{h}, && (15)
\end{aligned}$$

where we defined

$$Q\stackrel{def}{=}\phi_e-\frac{p_e}{k\rho},\quad \frac{1}{k}\stackrel{def}{=}\frac{cm_i}{q\sqrt{4\pi\rho}}, \tag{16}$$

and $\nu_m=c^2/4\pi\sigma$ is the magnetic diffusivity. Since $\mathbf{v}$ and ω are solenoidal fields we have

$$\operatorname{curl}(\omega\times\mathbf{v})=\mathbf{v}.\operatorname{grad}\omega-\omega.\operatorname{grad}\mathbf{v}=\{\mathbf{v},\omega\}, \tag{17}$$

TABLE I

Material	Conductivity σ (s^{-1})	Magnetic diffusivity ν_m ($cm^2\ s^{-1}$)	Speed U_o ($cm\ s^{-1}$)	Scale length L (cm)	Magnetic Reynolds number $R_m = LU_o/\nu_m$
Water + 25% NaCl (20 °C)	$1.9\ 10^{11}$	$3.7\ 10^{8}$	10^2	10^2	$2.7\ 10^{-5}$
Steel (molten, 1500 °C)	$6.3\ 10^{16}$	$1.1\ 10^{3}$	10	10^2	$8.8\ 10^{-1}$
Liquid Sodium (400 °C)	$5.4\ 10^{16}$	$1.3\ 10^{3}$	Industrial scales		10
Earth Core (10 °K)	$\sim 7\ 10^{17}$	$\sim 10^2$	10^{-1}	10^8	10^5
Plasmas	$\sim 8\ 10^{12}\ T^{3/2}$ (ev)	$\sim 8.9\ 10^{6} T^{3/2}$ (ev)	------	------	------
Solar Atmosphere ($\sim 10^4$ °K)	$\sim 8\ 10^{12}$	$\sim 10^7$	10^6	10^8	10^5
Solar plasma, higher altitude ($\sim$ 20 ev)	$\sim 8\ 10^{12}$	$\sim 10^5$	10^5	10^7	10^7
Plasma Focus ($\sim$ 2 Kev)	$\sim 7.6\ 10^{17}$	$\sim 10^2$	10^7	0.1	10^4
Copper (Solid, 20°C)	$5.4\ 10^{17}$	$1.3\ 10^{2}$	------	------	------

where $\{\mathbf{v}, \omega\}$ is the commutator of the vector fields $\mathbf{v}$ and ω. The contravariant component of the commutator is given in any curvilinear coordinate system by

$$\{\mathbf{v}, \omega\} = v^j \frac{\partial \omega^i}{\partial x^j} - \omega^j \frac{\partial v^i}{\partial x^j}, \tag{18}$$

provided the contravariant components v^i, ω^i, are used here. Integrability of Eqs. (14)–(15) requires that the curl of the rhs be zero. Thus eliminating P and Q we obtain

$$\frac{\partial \omega}{\partial t} + \{\mathbf{v}, \omega\} + \nu \operatorname{curl}\operatorname{curl}\omega = \{\mathbf{h}, \mathbf{J}\}, \tag{19}$$

$$\frac{\partial \mathbf{h}}{\partial t} + \{\mathbf{v}, \mathbf{h}\} + \nu_m \operatorname{curl}\operatorname{curl}\mathbf{h} = -\frac{1}{k}\{\mathbf{h}, \mathbf{J}\}. \tag{20}$$

The first two terms in these equations form the *convected time flux derivative*

$$\frac{D\omega}{Dt} \stackrel{def}{=} \frac{\partial \omega}{\partial t} + \{\mathbf{v}, \omega\},$$

which is a Lie derivative in an Euclidean spatio-temporal space $(t, \mathbf{x})$.[45] When dissipative terms are negligible and Hall's term is ignored ($1/k \to 0$), Eq. (20) is equivalent to

$$\frac{D\mathbf{B}}{Dt} = 0,$$

the equation for the conservation of the magnetic flux in ideal MHD. When Hall's effect is retained, but $\nu = \nu_m = 0$, adding Eqs. (19)–(20) we get

$$\frac{D(\omega + \Omega)}{Dt} = 0, \tag{21}$$

where $\Omega = k\mathbf{h} = q\mathbf{B}/m_i c$. This equation expresses the invariance of the flux of $\omega + \Omega$ in the so-called Hall-MHD.[56]

II.3 Stream function and magnetic flux function

Since $\operatorname{div}\mathbf{v} = 0$ and $\operatorname{div}\mathbf{h} = 0$ we can represent $\mathbf{v}$ and $\mathbf{h}$ locally as

$$\mathbf{v} = \operatorname{grad}\xi \times \operatorname{grad}\zeta, \tag{22}$$

$$\mathbf{k} = \operatorname{grad}\psi \times \operatorname{grad}\chi, \tag{23}$$

where ξ, ζ, ψ, and χ are called Euler potentials. The Euler representation is discussed in Refs. [30,45,53]. The flux of $\mathbf{v}$ (and, similarly, of $\mathbf{h}$) through any open surface S bounded by a closed contour C is given by

$$\int_S \mathbf{v}.d\mathbf{S} = \oint_C \xi d\zeta = -\oint_C \zeta d\xi \tag{24}$$

The special choices (i) $\zeta = z$, $\xi(x, y)$ and (ii) $\zeta = \theta$, $\xi(r, z)$ (similarly $\chi = z$, (i)$\psi(-x, y)$ or, (ii) $\psi(r, z)$) give

the stream function (and magnetic flux function) representation for planar symmetric motions and for axial symmetric flows, respectively. For (i) we have in Cartesian coordinates

$$v_x = \frac{\partial \xi}{\partial y}, \qquad v_y = -\frac{\partial \xi}{\partial x},$$
$$h_x = \frac{\partial \psi}{\partial y}, \qquad h_y = -\frac{\partial \psi}{\partial x},$$

and Eq.(24) shows that $[\xi(x_2, y_2) - \xi(x_1, y_1)]z$ or $[\psi(x_2, y_2) - \psi(x_1, y_1)]z$ are the fluxes of $\mathbf{v}$ and $\mathbf{h}$, respectively, through a surface spanned by any line segment joining (x_1, y_1) and (x_2, y_2) and a segment of height z. For (ii)

$$v_{<r>} = \frac{1}{r}\frac{\partial \xi}{\partial z}, \qquad v_{<z>} = -\frac{1}{r}\frac{\partial \xi}{\partial r},$$
$$h_{<r>} = \frac{1}{r}\frac{\partial \psi}{\partial z}, \qquad h_{<z>} = -\frac{1}{r}\frac{\partial \psi}{\partial r},$$

for the physical components of $\mathbf{v}$ in cylindrical coordinates. From Eq.(24) it follows that $2\pi\xi(r, z)$ and $2\pi\psi(r, z)$ are the fluxes of $\mathbf{v}$ and $\mathbf{h}$, respectively, through a disk of radius r, lying on the z = const. plane.

A considerable reduction of the set of six equations (19)–(20) is achieved when the configuration has an ignorable coordinate,[20] and is outlined in the Appendix.

II.4 Reduced MHD equations with translatory and rotational symmetry

It is convenient to write down the special cases that are needed in the paper, using the equations of the Appendix. We consider first cases with planar symmetry so that $ds^2 = (l_\alpha d\alpha)^2 + (l_\beta d\beta)^2 + dz^2$, $l_\gamma = 1$ and γ stands for the z cartesian coordinate. The $\mathcal{D}^2$ coincides with the two-dimensional Laplacian ∇^2, that is

$$\nabla^2 \xi = \operatorname{div} \operatorname{grad} \xi = \frac{l_\alpha}{l_\beta}\left[\frac{\partial}{\partial \alpha}\left(\frac{l_\beta}{l_\alpha}\frac{\partial \xi}{\partial \alpha}\right) + \frac{\partial}{\partial \beta}\left(\frac{l_\alpha}{l_\beta}\frac{\partial \xi}{\partial \beta}\right)\right]. \tag{25}$$

The equations for the MHD flows are

$$\left(\frac{\partial}{\partial t} - \nu \nabla^2\right)\nabla^2 \xi = \frac{1}{\sqrt{g}}\left([\nabla^2 \psi, \psi] - [\nabla^2 \xi, \xi]\right), \tag{26}$$
$$\left(\frac{\partial}{\partial t} - \nu \nabla^2\right) v_z = \frac{1}{\sqrt{g}}\left([\xi, v_z] - [\psi, h_z]\right), \tag{27}$$
$$-\frac{\partial \psi}{\partial t} = -\nu_m \nabla^2 \psi - \frac{1}{\sqrt{g}}\left([\xi, \psi] + -\frac{1}{\sqrt{g}} - [h_z, \psi]\frac{1}{k}\right), \tag{28}$$
$$\left(\frac{\partial}{\partial t} - \nu_m \nabla^2\right) h_z = \frac{1}{\sqrt{g}}\left([\xi, h_z] - [\psi, h_z]\right) - \frac{1}{\sqrt{g}}\left([\psi, \nabla^2 \psi]\right)\frac{1}{k}. \tag{29}$$

For cartesian coordinates $g = l_\alpha = l_\beta = 1$, and

$$[\xi, \psi] = \frac{\partial \xi}{\partial x}\frac{\partial \psi}{\partial y} - \frac{\partial \xi}{\partial y}\frac{\partial \psi}{\partial x}.$$

Here

$$\delta^* = dx\frac{\partial}{\partial y} - dy\frac{\partial}{\partial x},$$

and we find

$$dP = -\delta^*\left(\frac{\partial}{\partial t} - \nu \nabla^2\right)\xi + \nabla^2 \xi\, d\xi + d\frac{v_z^2}{2} - \nabla^2 \psi\, d\psi - d\frac{h_z^2}{2}. \tag{30}$$

Note that when considering steady state cases we can always set, for example, $\psi = -E_z t + \psi_0(\alpha, \beta)$, where E_z is a constant electric field, so that a constant may appear in the lhs of Eq. (28). Similar considerations apply to other equations.

Consider now the case of axial symmetric MHD flows written in cylindrical coordinates. Omitting the Hall effect for simplicity, $1/k = 0$, we have in this case,

$$\alpha = z, \quad \beta = r, \quad \gamma = \varphi, \quad l_\alpha = l_\beta = 1, \quad l_\varphi = r, \quad \sqrt{g} = r,$$

and

$$\mathcal{D}^2 = \frac{\partial^2}{\partial z^2} + r\frac{\partial}{\partial r}\left(\frac{1}{r}\frac{\partial}{\partial r}\right), \quad [f,g] = \frac{f}{z}\frac{g}{r} - \frac{f}{r}\frac{g}{z}.$$

The reduced equations are

$$\frac{1}{r^2}\left(\frac{\partial}{\partial t} - \nu\,\mathcal{D}^2\right)\mathcal{D}^2\xi = \frac{1}{r}\left([\frac{1}{r^2}\mathcal{D}^2\psi,\psi] + [\frac{1}{r^2},\frac{h_\varphi^2}{2}] - [\frac{1}{r^2}\mathcal{D}^2\xi,\xi] - [\frac{1}{r^2},\frac{v_\varphi^2}{2}]\right), \tag{31}$$

$$\left(\frac{\partial}{\partial t} - \nu\,\mathcal{D}^2\right)v_\varphi = \frac{1}{r}\left([h_\varphi,\psi] - [v_\varphi,\xi]\right), \tag{32}$$

$$\left(\frac{\partial}{\partial t} - \nu_m\,\mathcal{D}^2\right)\psi = \frac{1}{r}[\xi,\psi], \tag{33}$$

$$\frac{1}{r^2}\left(\frac{\partial}{\partial t} - \nu_m\,\mathcal{D}^2\right)h_\varphi = \frac{1}{r}\left([\xi,\frac{h_\varphi}{r^2}] - [\psi,\frac{v_\varphi}{r^2}]\right). \tag{34}$$

In addition, we have for $P = (p/\rho) + |\mathbf{v}|^2/2 + V$,

$$\delta^* = \frac{1}{r}\left(dz\frac{\partial}{\partial r} - dr\frac{\partial}{\partial z}\right)$$

and

$$dP = -\delta^*\left(\frac{\partial}{\partial t} - \nu\,\mathcal{D}^2\right)\xi + \frac{1}{r^2}\left(\mathcal{D}^2\xi\,d\xi + d\frac{v_\varphi^2}{2}\right) - \frac{1}{r^2}\left(\mathcal{D}^2\psi\,d\psi + d\frac{h_\varphi^2}{2}\right).$$

Here, the physical components for $\gamma = \varphi$ are $v_{<\varphi>} = v_\varphi/r$, $h_{<\varphi>} = h_\varphi/r$.

III. Dissipation of Magnetic Fields Enhanced by Plasma Flows

III.1 Enhanced dissipation: basic mechanism

A flow that near the stagnation point is approximated by $v_x = ax, v_y = -ay$, carries the magnetic lines (which lie parallel to the x axis) towards $y = 0$. (see Fig. 1) The evolution of the magnetic field, $B_x = B(y,t)$ is studied starting from an initial seed field $B(y,0)$.[9] The magnetic field equation is

$$\frac{\partial B}{\partial t} - \nu_m\frac{\partial^2 B}{\partial y^2} = \frac{\partial}{\partial y}(fB), \tag{35}$$

where $f = -ay$. A lateral gradient $\partial p/\partial x = -\rho C x$ is the driver of the motion and characterizes the strength of the stagnation flow, $a = \sqrt{C}$. It represents the pressure drop from the central channel of the squeezed plasma to a larger outlet volume in the surroundings. This flow and magnetic field are a particular exact solution of the MHD equations with resistivity and Hall effect in Ohm's law (see Sections II and IV).

Assuming that the field extends initially up to a distance h_o (on both sides) from $y = 0$, with the speed $U_o = ah_o$ we may define a magnetic Reynolds number $R_m = U_o h_o/\nu_m$. For large R_m diffusion is negligible over most of the slab $|y| \le h_0$, except in a small inner layer $|y| \le \delta$. The size of the resistive layer can be estimated setting the speed of the diffusion process, ν_m/δ, equal to the speed of advection of the magnetic field, $|v_y| = a\delta$. Hence $\delta/h_o = 1/\sqrt{R_m}$. From $|y| = h_o$ to $|y| = \delta$ the field is almost 'frozen–in', so that for the x component we get

$$B_t = B_o\frac{\delta x}{\delta x_o},$$

where B_t and δx are, respectively, the magnetic field and the line element at time t, corresponding to the initial values B_o and δx_o. Since the trajectories of the

plasma elements are given by

$$x = x_o \mathrm{e}^{at} , \qquad y = y_o \mathrm{e}^{-at} ,$$

we get

$$B(\delta, t) = B(y_o, 0)\frac{h_o}{\delta} = B(y_o, 0)\sqrt{R_m} . \tag{36}$$

This gives the order of magnitude of the amplification process, which is due to the 'stretching', $\partial x/\partial x_o$, of the magnetic lines, as they are convected to the resistive layer.[17]

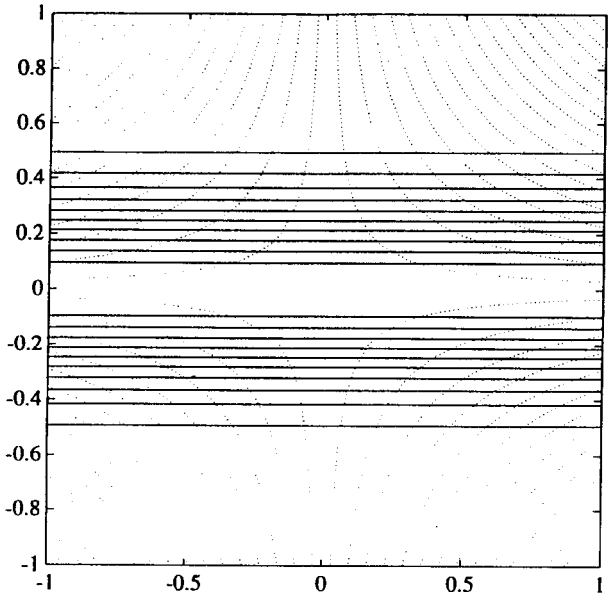

Figure 1. Stagnation point flow and magnetic field lines.

From the previous estimates it follows that the magnetic energy (per unit area) at the maximum amplification is (in order of magnitude)

$$W_M \approx \frac{B_M^2}{8\pi}\delta \approx W_o\sqrt{R_m} , \tag{37}$$

where $W_o \approx h_o B_o^2/8\pi$ is an estimate of the initial energy content. We assume that most of the energy is in a slab of size δ. When this energy level has been achieved the dissipation is, roughly, W_M per $1/a$ time units. The characteristic time for this enhancement is given by $(h_o/\delta \approx \exp(at_M))$,

$$at_M \approx \frac{1}{2}\ln R_m . \tag{38}$$

Energy dissipation reaches the highest rates at about this time too. Compared with the diffusion time in the absence of motion, $t_D = h_o^2/\nu_m$, we have

$$\frac{t_M}{t_D} \approx \frac{\ln R_m}{2R_m} . \tag{39}$$

The initial energy in a volume $V_o = h_o L_x L_z$ is $W_o = (B_o^2/8\pi)V_o$. This energy is both concentrated and augmented, so that one gets $W = W_o\sqrt{R_m}$, with an energy density $w = w_o R_m$ in a very small volume V_f. Therefore, the estimates of the energy per particle may reach very high values, i. e., $\Theta = (2/3)(w_o/n)R_m$.

III.2 Intensification and fast decay

The plausibility of a fast and intense dissipation of magnetic fields in a plasma can also be shown by a simple solution that describes the evolution of one Fourier component of the initial field.

As the motion starts, there is a stray initial magnetic field,

$$B(y, 0) = b_o \sin(k_o y) \tag{40}$$

Trying the solution

$$B(y, t) = b(t)\sin[k(t)y] , \tag{41}$$

we obtain

$$B(y, t) = b_o \sin(k_o \mathrm{e}^{at} y)\exp[at - \frac{1}{2R_m}(\mathrm{e}^{2at} - 1)] . \tag{42}$$

Here we have introduced an arbitrary length h_o, the size of the stagnation flow region in the y direction, so that we may define a characteristic inflow speed, $|v_y| = U_o = ah_o$, and a magnetic Reynolds number $R_m = h_o^2 a/\nu_m$. The initial field amplitude is first augmented to a maximum value

$$b_M = b_o\sqrt{R_m}\exp[-\frac{1}{2} + \frac{1}{2R_m}] \approx b_o\sqrt{\frac{R_m}{\mathrm{e}}} , \tag{43}$$

in a time

$$at_M = \frac{1}{2}\ln R_m - \ln(h_o k_o) , \tag{44}$$

followed by a decline, where the magnetic field extinguishes like $\exp[-(k_o^2\nu_m/a)\exp(2at)]$, as $t \to \infty$.

This case shows two basic trends which are common to all solutions: i) the magnetic field amplification

scales with $\sqrt{R_m}$; ii) the characteristic time for the intensification (which is accompanied by enhanced dissipation) scales with $\ln R_m/2a$. This is a few times (≈ 3 to 9 for R_m from 10^3 to 10^8) the period for traversing the distance h_o at the speed U_o, and is rather insensitive to changes in the resistivity of the plasma. In the absence of flow the magnetic field eq.(42) would decay over times of the order $t_d = 1/\nu_m k_o^2$, the classic diffusion time. The flow then accelerates the decay by a factor of the order $t_d/t_M \approx 2R_m/\ln R_m$.

We compute the magnetic energy in a cell of one wavelength size so that we may compare the total energy dissipated in it (from $t = 0$ to $t = \infty$) d, say, with the initial energy content, $\epsilon_o = (\pi/k_o)(b_o^2/8\pi)$. We find for large R_m

$$\frac{d}{\epsilon_o} \approx \frac{\sqrt{\pi R_m}}{h_o k_o}. \tag{45}$$

Summing up, this example indicates that in a time roughly estimated by $T = (1/2a)\ln R_m$, a plasma with a seed magnetic energy ϵ_o (per unit area) may receive near $\sqrt{\pi R_m}\epsilon_o$ in Joule heating. This energy is delivered mainly in a slab of size $\delta \approx (2\pi/k_o)\exp(-at_M) = (2\pi/k_o)\sqrt{R_m}$ in the y direction and a unit area.

III.3 Influence of the transients of the stagnation flow

If we consider time dependent flows of the type

$$f = a(t)y\,, \tag{46}$$

then one can see (from the equations of Section IV.1) that $a(t)$ satisfies the equation

$$\dot{a} = C - a^2 \tag{47}$$

If the gradient $\partial p/\partial x$ ceases to act at $t = 0$, the motion decays rather slowly, starting from a rate $a_o = \sqrt{C}$, according to the law

$$a(t) = \frac{a_o}{1 + a_o t}\,. \tag{48}$$

It can be shown that the evolution of a Fourier component like

$$B(y,t) = b(t)\sin[k(t)y]$$

is given by

$$k(t) = \frac{k_1}{1 + a_o t} \tag{49}$$

$$b(t) = \frac{b_1}{1 + a_o t}\exp[-\frac{(h_o k_1)^2}{R_m}\frac{a_o t}{1 + a_o t}] \tag{50}$$

where k_1, b_1 are the values for $t = 0$. The decay of the magnetic field takes place over a period of many times $1/a_o$. We may note that if the action of the gradient stops ($C = 0$) at the time of maximum enhancement of the magnetic field a period given by $a_o t \approx (R_m/\mathrm{e})^{1/2}$ must pass before the field decays to the original values. The dissipation will still be relevant during several times $1/a_o$ after the switch off of $\partial p/\partial x$, since the mechanism of stretching of the magnetic lines continues to act for some time, although slowly weakening. As a consequence, a magnetic field highly localized in a region of size $\delta = h_o/\sqrt{R_m}$ which would decay in a time $\tau_d \approx \delta^2/\nu_m = 1/a_o$ (a transit time) in the absence of a flow, extinguishes instead over the much longer time $\tau_d\sqrt{R_m}$ during the decline of the motion.

IV. Build up of current sheets

IV.1 Planar flow and magnetic field evolution

The results presented here[18] rely on a solution of the reduced MHD equations (Section II.4) of the form

$$\xi = xf(y,t) \qquad \psi = \psi(y,t) \tag{51}$$

(ξ, χ: stream function and magnetic flux, respectively; $v_y = -\partial_x\xi, B_x \equiv B = \partial_y\chi$) which has a stagnation point at the origin when $f(0,t) = 0$. The flow (see Eq. (26)) is ruled by the equation

$$\nu f''' = -C + f'^2 - ff'' + \frac{\partial f'}{\partial t} \tag{52}$$

where C is a constant that measures the pressure gradient in the x direction, and f' is a shorthand for $\partial f/\partial y$, and ν is the viscous diffusivity.

This configuration with planar symmetry, where z is the ignorable variable, can be extended by the inclusion

of a $B_z = D(y,t)$ component. (see Fig. 2) Thus, the MHD equations allow the following (exact) reduction

$$v_x = xa(t) \quad v_y = -ya(t) \quad v_z = 0 \tag{53}$$

$$B_x = B(y,t) \quad B_y = 0 \quad B_z = D(y,t) \tag{54}$$

$$\frac{\partial}{\partial x}(\frac{p}{\rho}) = -C(t)x\ . \tag{55}$$

Equation (52) gives $\dot{a} = C - a^2$, which determines the rate $a(t)$ of the stagnation flow when the pressure gradient (per unit length) C along the current sheet is given. Equation (30) completes the determination of the pressure field as

$$\frac{p}{\rho} + \frac{B^2 + D^2}{8\pi\rho} = \frac{p_o}{\rho} + \frac{1}{2}C(t)(y^2 - x^2) - a(t)^2 y^2 \tag{56}$$

$$\tag{57}$$

For the magnetic field evolution we find (from Eqs. (28) and (29))

$$\frac{\partial B}{\partial t} = \frac{\partial}{\partial y}(ayB) + \nu_m \frac{\partial^2 B}{\partial y^2} \tag{58}$$

$$\frac{\partial D}{\partial t} = ay\frac{\partial D}{\partial y} + \nu_m \frac{\partial^2 D}{\partial y^2}\ . \tag{59}$$

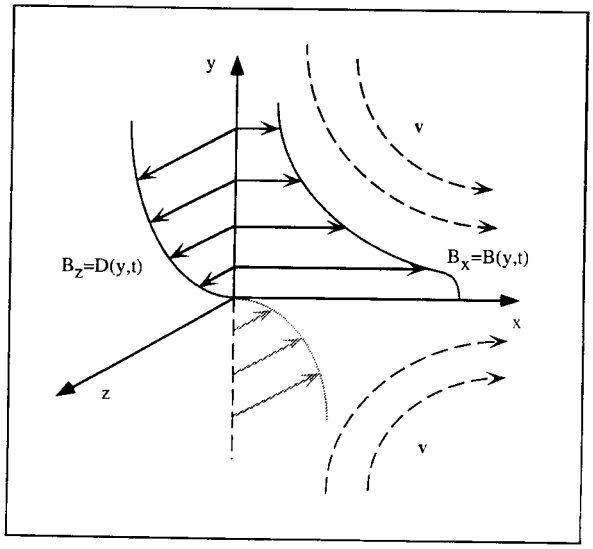

Figure 2. Magnetic field components in the planar flow model.

These equations are valid under the complete Ohm equation (3) although, due to the particular space dependence of the solution, the Hall term does not contribute. Note that equation (58) besides advection includes an amplification effect for B. This is due to the magnetic line stretching provided by the v_x component. The component D does not show this effect. Equation (58) implies the conservation of the total magnetic flux $F = \int_{-\infty}^{\infty} B dy$ in time when B decreases faster than $1/|y|$ as $|y| \to \infty$, i. e., no flux injection. Thus, although the system is dissipative, F is an invariant when there is no flux injection. The evolution of the x magnetic field component is studied starting from a given initial distribution of stray or seed field $B(y,0)$. For a simple irrotational flow

$$f = ay \tag{60}$$

$(a = \sqrt{C})$ the transformation of variables

$$\zeta = \frac{y}{h_o}e^{at} \quad \tau = \frac{1}{2R_m}(e^{2at} - 1) \quad B^*(\zeta,\tau) = \mathrm{e}^{-at}h_o B(y,t)$$

leads to the diffusion equation

$$\frac{\partial B^*}{\partial \tau} = \frac{\partial^2 B^*}{\partial \zeta^2}\ . \tag{61}$$

Here we have introduced a scale length, h_o, for the region size so that the characteristic inflow speed is $|v_y| = U_o = h_o a$, and a magnetic Reynolds number $R_m = h_o^2 a/\nu_m$ can be defined. In the following discussion R_m is assumed to be large.

IV.2 General solution of the initial value problem.

Knowing the initial field $B^*(\zeta,0) = h_o B(y,0)$ the Poisson integral gives B^* at a later time as

$$B^*(\zeta,\tau) = \frac{1}{2\sqrt{\pi\tau}}\int_{-\infty}^{\infty} \mathrm{e}^{-(\zeta-\xi)^2/4\tau} B^*(\xi,0)d\xi\ . \tag{62}$$

Alternatively we may use the Fourier transform of the initial condition

$$\varphi(k,0) = \mathcal{F}_k\{B^*(\zeta,0)\} = \frac{1}{\sqrt{2\pi}}\int_{-\infty}^{\infty} \mathrm{e}^{-i\zeta k} B^*(\zeta,0)d\zeta\ . \tag{63}$$

Then we can compute $B^*(\zeta,\tau)$ with the formula

$$B^*(\zeta,\tau) = \frac{1}{\sqrt{2\pi}}\int_{-\infty}^{\infty} \varphi(k,0)\mathrm{e}^{-i\zeta k}\mathrm{e}^{-k^2\tau}dk\ . \tag{64}$$

Applying Parseval's identity we obtain the total magnetic energy (per unit area) as a function of time

$$W(t) = \int_{-\infty}^{\infty} dy \frac{|B^*(y,t)|^2}{8\pi} = \int_{-\infty}^{\infty} dk \frac{h_o}{8\pi} |\varphi(k,0)|^2 e^{at-(1/R_m)(h_o k)^2(e^{at}-1)} . \quad (65)$$

Setting

$$W(t) = \int_{-\infty}^{\infty} \frac{B^2}{8\pi} dy$$

for the total magnetic energy per unit area in the x, z plane, we can compute the energy dissipated by Joule heating in the system (per unit cross section in x, z) from $t = 0$ to a time t as

$$D(t) = \int_0^t dt \int_{-\infty}^{\infty} \frac{j^2}{\sigma} dy = a \int_0^t W(t')dt' - [W(t) - W(0)] . \quad (66)$$

Thus, knowledge of $W(t)$, the magnetic energy as a function of time, is sufficient to obtain the energy dissipated in a given period.

IV.3 Solutions without flux injection

The magnetic field equation for the irrotational flow is invariant under $y \to -y$ exchange, thus it allows for solutions with definite parity in y. Consider first the case of initial magnetic fields with finite (total) flux (per unit length)

$$F = \int_{-\infty}^{\infty} B(y,0)dy . \quad (67)$$

Thus we require $B(y,0)$ that goes to zero faster than $1/|y|$ as $|y| \to \infty$. For these cases $v_y B \to 0$ as $|y| \to \infty$, so that there is no inflow of magnetic field flux from far away borders. From the Poisson integral it can be proved that

$$\lim_{t\to\infty} B(y,t) = \sqrt{\frac{R_m}{2\pi}} \frac{1}{h_o} \exp[-\frac{R_m}{2}(\frac{y}{h_o})^2]F \quad (68)$$

from which we conclude:

The odd solutions originated by initial magnetic fields integrable in absolute value in $(-\infty, \infty)$ decay asymptotically as $t \to \infty$ ($F = 0$). The corresponding even solutions tend all to the Gaussian form eq. (68) ($F \neq 0$).

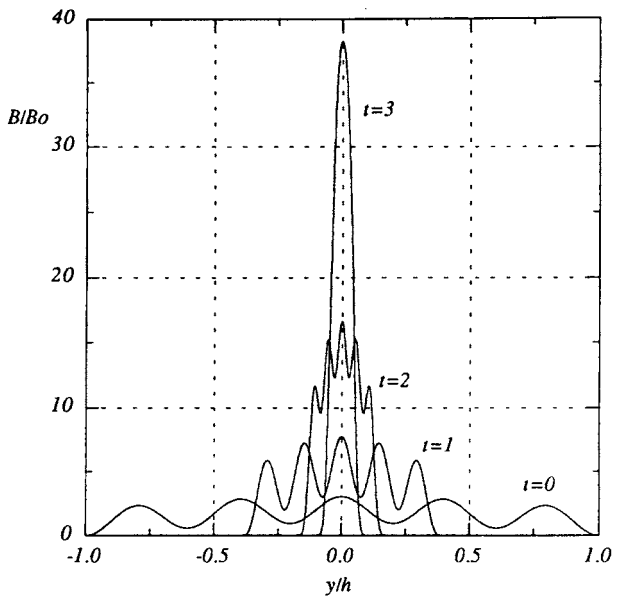

Figure 3. Evolution of a rippled initial magnetic field.

Therefore, when no magnetic flux is supplied from the outside, we may expect that the odd part of a seed magnetic field will be amplified first and finally completely dissipated. An even part, instead, will be amplified and concentrated in a thin layer of (half height) width $\delta/h_o = 1.177/\sqrt{R_m}$. This is illustrated in Fig. 3 where a rippled magnetic field is added to an even initial condition. The intensity of the magnetic field in

this filament reaches the peak value $\sqrt{R_m/2\pi}F/h_o = \sqrt{a/2\pi\nu_m}F$. If the even magnetic field existed initially only in a y interval of width h_o, the initial mean value of the magnetic field F/h_o produces a peak value $\sqrt{R_m/2\pi}$ times larger in the final state. The magnetic filament persists for as long as the flow continues, keeping an exact balance between amplification, transport, and diffusion.

IV.4 Magnetic amplification and decay of an odd solution

The case of odd initial distributions of magnetic field which oscillate in space and are modulated by a Gaussian of the type

$$B(y,0) = b_o s \exp[-\frac{s^2}{2}(\frac{y}{h_o})^2]\sin(\tilde{k}y) \tag{69}$$

is amenable to explicit solution formulas using the Fourier technique.

For the odd initial condition we obtain

$$\frac{W(t)}{W(0)} = g(t)\mathrm{e}^{at}\frac{\exp(g^2h_o^2\tilde{k}^2/2s^2)-1}{\exp(h_o^2\tilde{k}^2/2s^2)-1}\,, \tag{70}$$

where

$$g(t) = \frac{\sqrt{R_m}}{s}\left(1+[(R_m/s^2)-1]\mathrm{e}^{-2at}\right)^{-1/2}\mathrm{e}^{-at}, \tag{71}$$

and the limit for $t\to\infty$ is zero. The odd field extinguishes completely. However, before that, an amplification stage takes place, and considerable amounts of energy can be dissipated during the whole process for $R_m >> 1$. When $(h_o\tilde{k}/2s)^2 << 1$, the initial field is approximately

$$B(y,0) = 2sb_o\tilde{k}y\exp[-(s^2/2)(y/h_o)^2] \tag{72}$$

(proportional to the derivative of the Gaussian) which shows two main peaks of opposite magnetic intensity. The energy evolution is then

$$\frac{W(t)}{W(0)} = g(t)^3\mathrm{e}^{at}\,. \tag{73}$$

The time t_M for the maximum energy amplification is given (for $R_m >> 1$) by

$$at_M = \frac{1}{2}\ln\frac{R_m}{2s^2} - \frac{1}{2}\ln 2\,, \tag{74}$$

with a maximum energy

$$\frac{W(t_M)}{W(0)} = \frac{2\sqrt{R_m}}{3^{3/2}s}\,. \tag{75}$$

The extinction takes place in a few transit times $1/a$, after t_M.

IV.5 Evolution of the magnetic field component normal to the flow.

The component $B_z = D(y,t)$ of the magnetic field (Fig. 2) is ruled by Eq. (59). The evolution is very different to that of the B_x component: there is no amplification and all the solutions without flux injection vanish. Assuming that $D\sim 1/|y|^{1+e}$, $e>0$, so that the total flux integral exists $F=\int_{-\infty}^{\infty}D\,dy$, and $ayD\to 0$ for $|y|\to\infty$, from Eq. (59) follows

$$\frac{\partial F}{\partial t} = -aF. \tag{76}$$

Thus all even solutions ($F\neq 0$) are extinguished in a few units of $1/a$ as $F = F_0\exp(-at)$. All odd initial magnetic fields have $F(0)=0$, and F is invariant and remains null for these solutions. However, multiplying Eq. (59) by D and integrating, we derive (for zero flux injection)

$$\frac{\partial}{\partial t}\int_{-\infty}^{\infty}\frac{D^2}{8\pi}dy = -a\int_{-\infty}^{\infty}\frac{D^2}{8\pi}dy - \frac{1}{4\pi\nu_m}\int_{-\infty}^{\infty}\left(\frac{\partial D}{\partial y}\right)^2 dy, \tag{77}$$

which shows that the magnetic energy decays, so that the odd solution also dies. Two steady state solutions are the exception,

$$D = D_0 = const., \qquad D = \frac{2D_1}{\sqrt{\pi}}\int_0^{\sqrt{a/\nu_m}\,y} e^{-\xi^2}d\xi,$$

but, of course, for these cases the flux and energy integrals do not exist. These solutions are sustained by a continuous flux injection from the outside. In fact, we may note that, asymptotically, $|v_y D| \sim |ayD_{0,1}|$ for these solutions, which means that, far away from the stagnation point where v_y takes a constant value, the magnetic field must increase linearly. In other words, the steady state solutions are supported by an increasing magnetic flux injection from the plasma mainstream (see also Section VII.1). As soon as the flux injection decreases or returns to a constant rate, these magnetic fields begin to decline. The initial value problem for D can be solved in general by transforming Eq.(59) into the form

$$\frac{\partial D}{\partial \tau} = \frac{\partial^2 D}{\partial \zeta^2} \tag{78}$$

by the change of variables

$$\zeta = \frac{y}{y_0}\mathrm{e}^{a\,t}, \qquad \tau = \frac{1}{2R_m}\left(\mathrm{e}^{2a\,t} - 1\right).$$

Then, the Poisson integral, Eq.(62), or the Fourier formula Eq. (64) can be applied.

V. The Energetics of the Current Sheet

V.I Magnetic energy

From the Maxwell equations and Ohm's law, the variation of magnetic energy is given as[45]

$$\frac{\partial}{\partial t}\frac{|B|^2}{8\pi} = -\mathrm{div}\,(\frac{c}{4\pi}\mathbf{E}\times\mathbf{B}) - \frac{1}{c}(\mathbf{j}\times\mathbf{B}).\mathbf{v} - \frac{1}{\sigma}|\mathbf{j}|^2\,. \tag{79}$$

On the other hand, from the MHD equations of motion the kinetic energy change is given by

$$\frac{\partial}{\partial t}(\frac{1}{2}\rho|\mathbf{v}|^2) = -\mathrm{div}\,\left\{\mathbf{v}(p + \frac{1}{2}\rho|\mathbf{v}|^2 - \eta\mathrm{grad}\,\frac{|\mathbf{v}|^2}{2})\right\} + \frac{1}{c}(\mathbf{j}\times\mathbf{B}).\mathbf{v} - \epsilon_\eta\,, \tag{80}$$

where

$$\epsilon_\eta \equiv \eta\frac{\partial v_k}{\partial x_j}\frac{\partial v_k}{\partial x_j}$$

is the viscous dissipation. When the velocity field is steady state, and eliminating the power of the Lorentz force we have

$$\frac{\partial}{\partial t}\frac{|B|^2}{8\pi} = -\mathrm{div}\,(\frac{c}{4\pi}\mathbf{E}\times\mathbf{B}) - \mathrm{div}\,\left\{\mathbf{v}(p + \frac{1}{2}\rho|\mathbf{v}|^2 - \eta\mathrm{grad}\,\frac{|\mathbf{v}|^2}{2})\right\} - \frac{1}{\sigma}|\mathbf{j}|^2 - \epsilon_\eta\,. \tag{81}$$

On the other hand, from equation (58), and considering the irrotational flow (53), after multiplication by B, integration over y, and integration by parts, we obtain

$$\frac{\partial}{\partial t}\int_{-\infty}^{\infty}\frac{|B|^2}{8\pi}dy = a\int_{-\infty}^{\infty}\frac{|B|^2}{8\pi}dy - \frac{\nu_m}{4\pi}\int_{-\infty}^{\infty}(\frac{\partial B}{\partial y})^2 dy \tag{82}$$

assuming that $B \to 0$ as $y \to \pm\infty$ at least as $1/y$. The first integral in the rhs gives the growth of magnetic energy provided by transport and stretching of the magnetic lines, and the second integral gives the loss due to Joule heating.

V.2 Energy augmentation and dissipation

To find the origin of the amplification term we may integrate the general equation (81) over a region $\mathcal{R}$ in the (x, y) plane. Note, that for the irrotational motion $\mathrm{div}\,(\eta\,\mathrm{grad}\,|\mathbf{v}|^2/2) - \epsilon_\eta = 0$, and that here the Poynting vector is

$$c\frac{\mathbf{E}\times\mathbf{B}}{4\pi} = \frac{c}{4\pi}E_z B_x \mathbf{e}_y \tag{83}$$

(where $\mathbf{e}_y$ is the unit vector in the y direction). Then

$$\frac{\partial}{\partial t}\int_{\mathcal{R}}\frac{B^2}{8\pi}dydx = -\oint_{\partial\mathcal{R}}\frac{c}{4\pi}E_z B_x \mathbf{e}_y.\mathbf{n}d\ell - \oint_{\partial\mathcal{R}}(\mathbf{v}.\mathbf{n})(p+\frac{1}{2}\rho|\mathbf{v}|^2)d\ell - \int_{\mathcal{R}}\frac{\nu_m}{4\pi}(\frac{\partial B}{\partial y})^2 dydx\ , \tag{84}$$

where $\mathbf{n}$ is the exterior normal on the boundary $\partial\mathcal{R}$, and $\mathrm{d}\ell$ is the corresponding differential length. The region $\mathcal{R}$ may be chosen as a rectangle centered on the origin, defined by $-L_x \le x \le L_x$, $-h_o \le y \le h_o$, then we let $h_o \to \infty$. We can see that the flux of the Poynting vector gives no contribution. Comparing eq. (82) with eq.(84) we find

$$\int_{-\infty}^{\infty} a\frac{B^2}{8\pi}dy.2L_x = \oint_{\partial\mathcal{R}}\frac{B^2}{8\pi}(\mathbf{v}.\mathbf{n})d\ell = -\oint_{\partial\mathcal{R}}(\mathbf{v}.\mathbf{n})(p+\frac{1}{2}\rho|\mathbf{v}|^2)d\ell\,. \tag{85}$$

(since $v_x|_{\pm L_x} = \pm aL_x$).

Thus the term which provides the amplification of the magnetic energy derives from the diminution of the net power exerted by the dynamic pressure $p+1/2\rho|\mathbf{v}|^2$ on the region considered. In fact, for the motion given by eq.(53), MHD Bernouilli's equation

$$p + \frac{1}{2}\rho|\mathbf{v}|^2 + \frac{B^2}{8\pi} = const. \tag{86}$$

holds (as can be seen from eq.(56)), and when the velocity field is invariant in time, any local intensification of $B^2/8\pi$ is at the expense of a local descent of the plasma pressure. It is clear that the cause of the current sheath build-up is the asymptotic dynamic pressure value. This is the cause of the squeezing of the fluid and the associated outflow. To operate, the model assumes the existence of pressure differences as large as needed.

VI. Self Similar Solutions

VI.1 Reduction to ordinary differential equations

Equation (58) with $f = ay$ admits an infinite set of solutions with self similarity.[18] It contains even and odd solutions without flux injection, and an odd solution with constant flux injection that approaches the steady state. Using the principle of superposition of solutions, many other examples can be worked out. Starting from Eq. (58) with $f = a(t)y$, so that $a(t)$ can in general be a function of t, one may search for a solution of the form

$$B(y,t) = b(t)H[\gamma(t)(y-\eta(t))]\ . \tag{87}$$

The self similar variable is $z = \gamma(t)[y-\eta(t)]$, where $\gamma(t), \eta(t)$ are functions of time to be determined, and $b(t)$ is the time-varying amplitude of the similarity solution. With this hypothesis one obtains that solutions exist for time functions $\gamma(t), b(t), \eta(t)$ such that

$$\frac{1}{\gamma^2\nu_m}(a - \frac{\dot\gamma}{\gamma}) = q \tag{88}$$

$$\frac{1}{\gamma^2\nu_m}(a - \frac{\dot b}{b}) = p \tag{89}$$

$$\frac{1}{\gamma\nu_m}(\dot\eta + a\eta) = k \tag{90}$$

where q, p, k are arbitrary constants. No generality is lost by taking $k = 0$ and $q = 1$, and setting $p \equiv \lambda + 1$, we get

$$\frac{\mathrm{d}^2 H}{\mathrm{d}z^2} + z\frac{\mathrm{d}H}{\mathrm{d}z} + (\lambda + 1)H = 0 \,, \qquad (91)$$

which leads to a solution in terms of parabolic cylinder functions.

When the plasma motion is in steady state, $a = const.$, we take $\tilde{\gamma} = h_o\gamma/\sqrt{R_m}$, and find

$$\tilde{\gamma}(t) = \frac{\tilde{\gamma}_o}{\sqrt{\tilde{\gamma}^2 + (1 - \tilde{\gamma}^2)\exp(-2at)}} \,, \qquad (92)$$

so that

$$b(T) = b_o \exp[-\lambda a t][\tilde{\gamma}_o^2 + (1 - \tilde{\gamma}_o^2)\exp(-2at)]^{-p/2} \,. \quad (93)$$

Thus, $b(t)$ grows without bound unless $p > 1$.

The time t_M where the maximum value of $b(t)$ is reached is given by

$$t_M = -\frac{1}{2}\ln\left[\frac{(p-1)\tilde{\gamma_o}^2}{1 - \tilde{\gamma_o}^2}\right] \,. \qquad (94)$$

The maximum value of $b(t)$ is, therefore,

$$b(t_M) = b_o\sqrt{\frac{1 - \tilde{\gamma_o}^2}{(p-1)\tilde{\gamma_o}^2}}\left[\frac{p-1}{p(1 - \tilde{\gamma_o}^2)}\right]^{p/2} \,. \qquad (95)$$

VI.2 Gaussian magnetic field and skew-symmetric magnetic field sustained by flux injection

When $\lambda = 0$ we find two important solutions, which can be checked directly by derivation,

$$H^{(e)}(z) = \exp(-\frac{z^2}{2}) \qquad \text{(even)} \qquad (96)$$

$$H^{(o)}(z) = \exp(-\frac{z^2}{2})\int_0^z \exp(\frac{\zeta^2}{2})d\zeta \qquad \text{(odd)} \quad (97)$$

The first equation gives Gaussian type magnetic fields, with changing intensity, spread, and peak position in time. These are solutions without flux injection, which all approach a Gaussian steady state centered at $y = 0$. The second one is Dawson's function and approaches the odd steady state supported by flux injection[49]. In fact, for $|z| \to \infty$, the asymptotic behaviour of this solution is z^{-1} so that $\lim |y| \to \infty\, yB$ is finite.

We can see that the case $\lambda = 0$ leads to the same time behaviour for $\tilde{\gamma}(t)$ and $b(t)$, i. e., $b(t) \propto \tilde{\gamma}(t)$. Starting with $\tilde{\gamma} >> 1$ for $T = 0$, corresponds to highly concentrated initial fields. Eq. (92) shows that $\tilde{\gamma}$ decreases very fast to the asymptotic limit $\tilde{\gamma} = 1$ as $T \to \infty$. The same happens with the amplitude b. In fact, we can obtain a Green's function, i. e., the delta function as initial condition, setting $\tilde{\gamma} = b_o = \infty$, so that initially $B(y, 0) = \delta(y - \eta_o)$.

Conversely, when $\tilde{\gamma} << 1$ for $T = 0$, we are considering initially very sparse fields. Now Eq. (92) shows that $\tilde{\gamma}$ grows until the limit value $\tilde{\gamma} = 1$ is approached as $T \to \infty$. In this case $b(T)$ grows also until the Gaussian steady state is obtained. This corresponds to the amplification process. For all values of γ the center of the self similar solution may change its position as time progresses. Thus, we can see, for example, that the center of the Gaussian, or the center of Dawson's function, tends towards $y = 0$ as $t \to \infty$. (See Fig. 4)

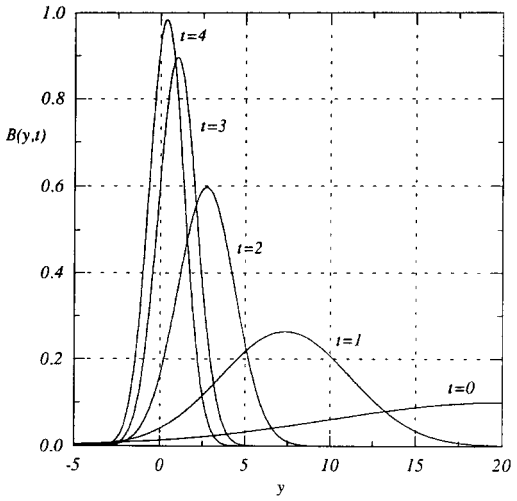

Figure 4. Time evolution of a Gaussian solution.

VI.3 Amplification and decay of Hermite solutions

From Eq. (96), by successive derivations, we may find an infinite subset of self similar solutions. In fact, if we derive Eq. (91) n times we obtain the same equation with $\lambda = n$. On the other hand, from the generating function of Hermite polynomials we have

$$\mathcal{H}_n(z)\mathrm{e}^{-\frac{z^2}{2}} = (-1)^n(\frac{\mathrm{d}}{\mathrm{d}z})^n\mathrm{e}^{-\frac{z^2}{2}} \,, \qquad (98)$$

where $\mathcal{H}_n(z)$ indicates the Hermite polynomial of order n. Thus

$$H(z) = \mathcal{H}_n(z)\mathrm{e}^{-\frac{z^2}{2}} \tag{99}$$

is a self similar solution with $p = (1+n)$, n arbitrary positive integer. It is basically of Gaussian type, modulated by oscillations of the magnetic field, according to the zeros of the polynomials. Since $\tilde{\gamma} \to 1$, b decays ($b \to 0$) as $t \to \infty$ as can be seen from (Eqs. (92)–(93)), for this subset of solutions. These are even and odd solutions, without flux injection (they decrease faster than $1/|y|$ as $|y| \to \infty$). All of them have total magnetic flux $F = 0$, so they all produce a transient, with intense energy dissipation for large R_m, and then die. (See Fig. 5)

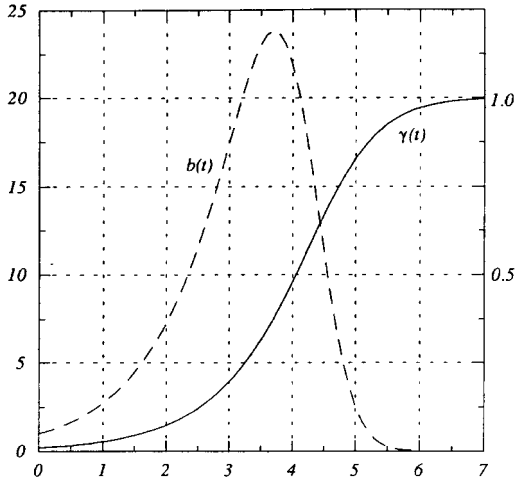

Figure 5. Self similar solutions for n=3.

The magnetic energy is given by

$$W(t) = W(0)\left[\frac{\mathrm{e}^{-2\lambda a t}}{\tilde{\gamma}_o^2 + (1-\tilde{\gamma}_o^2)\exp(-2at)}\right]^{(\lambda+1)/2} . \tag{100}$$

Thus, when $\lambda > 0$ the energy tends to zero as $t \to \infty$. The case $\lambda = 0$ gives $W(\infty) = W(0)/\tilde{\gamma}_o$.

VI.4 Self similar solutions for the normal magnetic field component

Equation (59) for $B_z = D(y,t)$ also allows self similar solutions. The magnetic field profiles are the same as those found for the B_x component, but their temporal behavior is different. The self similar solutions describe the extinction of the component normal to the flow. Writing $D = \beta(t)M(\xi)$ where $\xi = \gamma(t)(y - d(t))$ we find a set of differential equations for $\beta(t)$, $\gamma(t)$, $d(t)$, and $M(\xi)$. Let p, q, and r be three constants. We find,

$$\frac{\dot{\beta}}{\beta} = -r\nu_m\gamma^2, \tag{101}$$

$$\frac{\dot{\gamma}}{\gamma} = a - p\nu_m\gamma^2, \tag{102}$$

$$\dot{d} = -q\nu_m\gamma - a\,d, \tag{103}$$

$$M'' + M'(p\,\xi + q) + r\,M = 0, \tag{104}$$

for the similarity solutions. Setting $pr + \lambda + 1$ and $p\xi + q = \sqrt{p}z$, we obtain

$$\frac{\mathrm{d}^2M}{\mathrm{d}z^2} + z\frac{\mathrm{d}M}{\mathrm{d}z} + (\lambda+1)M = 0, \tag{105}$$

so that the solutions of Sections VI.2 and VI.3 apply. For $\lambda = n$ with $n = 1, 2, 3, \ldots$, we obtain the Hermite functions, Eq. (99), and for $\lambda = 0$ the Gaussian, Eq. (96), and the Dawson integral, Eq. (97) functions. The amplitude $\beta(t)$ of these solutions, however, decays to zero, as it is seen from Eq. (101).

VII. Formation of Current Sheets by Continuous Flux Injection

VII.1 Boundary conditions in driven systems

When $\lim_{|y|\to\infty} yB$ is not zero, an incoming flux is being added to the system by the plasma flow. This condition corresponds to a finite value for the flux rate v_yB, which in a realistic flow will be represented by constant incoming velocity and magnetic field at large distances. We can see that the diffusive term is asymptotically of decreasing importance, as it varies like $1/y^3$. Thus for large y, we have the 'freezing' of the magnetic field in the plasma,

$$\frac{\partial B}{\partial t} - ay\frac{\partial B}{\partial y} = aB\,, \quad (|y| \to \infty)\,. \tag{106}$$

Therefore

$$B(y,t) = F(y\mathrm{e}^{at})\mathrm{e}^{at} \tag{107}$$

gives the possible asymptotic behaviour for large y; here $F(Y)$ represents the spatial distribution of B, at an initial time $t = 0$ for large $|Y|$ values. Thus, depending on the configurations of distant magnetic fields the system may be driven in general by time-varying fluxes (even assuming the incoming plasma speed constant in time). The case $F(Y) = a_1/Y$ for positive Y, say, gives a flux injection constant in time, from that side $\lim_{y\to+\infty} yB = a_1 = \text{const.}$. This is the type of flux injection we consider here.

VII.2 Even solution: unbounded growth

An important point is to show that a system with unbalanced flux injection from positive and negative y sides, leads to a magnetic field which grows in time, never approaching a steady state. Assume an initial field $B(y,0) = B(y)$ such that $\lim_{y\to+\infty} yB_0 = a_1$, and $\lim_{y\to-\infty} yB_0 = a_1'$, with $a_1 \neq a_1'$. This initial condition can be split into odd and even parts

$$B_0^o = \frac{1}{2}(B_0(y) - B_0(-y))\,,$$
$$B_0^e = \frac{1}{2}(B_0(y) + B_0(-y))\,. \tag{108}$$

Then,

$$\lim_{y\to+\infty} yB_0^o = \frac{1}{2}(a_1 - a_1') \equiv \bar{a}_1\,, \tag{109}$$

and

$$\lim_{y\to+\infty} yB_0^e = \frac{1}{2}(a_1 + a_1') \equiv d\,. \tag{110}$$

We now divide B_0^e in a 'driven' or asymptotic part, and an initial 'seed', i. e.,

$$B_0^e = \frac{d}{|y|} + (B_0^e - \frac{d}{|y|})\,, \quad \text{for} |y| \geq h_0\,, \tag{111}$$

where $h_0 > 1$ is any finite distance to the origin, so that the 'driven' part is

$$B_0^{ed} = \frac{d}{|y|}\,, \quad \text{for} |y| \geq h_0\,,$$
$$B_0^{ed} = 0\,, \quad \text{for} |y| < h_0\,, \tag{112}$$

and the 'seed' is

$$B_0^{es} = B_0^e - \frac{d}{|y|}\,, \quad \text{for} |y| \geq h_0\,,$$
$$B_0^{es} = B_0^e\,, \quad \text{for} |y| < h_0\,. \tag{113}$$

Clearly, $\lim_{|y|\to\infty} yB_0^{es} = 0$, the 'seed' part is not sustained by flux injection, and therefore the properties derived in Section IV for a free system apply. Hence, this part of the solution tends to the gaussian profile, Eq. (68). The evolution of the driven part can be obtained using Poisson's integral, Eq. (62),

$$B^{ed}(y,t) = dh_0 \frac{\sqrt{\phi}}{\sqrt{\pi}} \int_{|y|>h_0} \frac{d\xi}{|\xi|} \exp[-(y-\chi\xi)^2\phi]\,, \tag{114}$$

where we have set $\xi = \mathrm{e}^{-at}$ and $\phi = a/(2\nu_m(1-\mathrm{e}^{-2at}))$. From this formula one gets

$$B^{ed}(y,t) = dh_0 \frac{\sqrt{\phi}}{\sqrt{\pi}} \mathrm{e}^{-y^2\phi} \int_{h_0}^{\infty} \frac{d\xi}{\xi} \exp[-\chi^2\phi\xi^2] 2\cosh(2y\chi\phi\xi)\,. \tag{115}$$

Since $\chi \to 0$ as $t \to \infty$ while $\phi \to a/2\nu_m$, the integral grows steadily as time elapses. In fact,

$$\int_{h_0}^{\infty} \frac{d\xi}{\xi} \exp[-\chi^2\phi\xi^2] = \frac{1}{2}\int_{\chi^2\phi h_0}^{\infty} \frac{d\zeta}{\zeta} \mathrm{e}^{-\zeta} = -\frac{1}{2}\mathrm{Ei}(-\chi^2\phi h_0^2) \tag{116}$$

where Ei is the exponential-integral function. The following property holds for $x > 0$

$$\mathrm{Ei}(-x) = C + \ln x - \int_0^x (1-\mathrm{e}^{-u})\frac{du}{u} \tag{117}$$

($C = 0.5772\ldots$, Euler's constant). Thus, we get

$$B^{ed}(y,t) \geq \frac{d}{h_0}\frac{\sqrt{\phi}}{\sqrt{\pi}} \mathrm{e}^{-y^2\phi} \left[-\ln(\chi^2\phi h_0^2) + \int_0^{\chi^2\phi h_0^2} (1-\mathrm{e}^{-u})\frac{du}{u} - C \right]\,, \tag{118}$$

a lower bound that grows linearly with time, for $\exp(at) >> 1$, as

$$B^{ed}(y,t) \geq \frac{d}{h_0}\sqrt{\frac{2R_m}{\pi}}\mathrm{e}^{-(R_m/2)(y/h_0)^2}at. \qquad (119)$$

This result has important physical consequences. We have seen that the odd fields tend to a unique steady state current sheet represented by Dawson's function, Eq. (97), as time goes by. This current sheet, similarly to what happens during a short transient with the odd fields of non driven systems, is also reduced to a thin layer and shows two peaks of magnetic fields with opposite sign, whose intensity scales with $\sqrt{R_m}$, for $R_m >> 1$. The odd driven current sheet, as well as the even nondriven part of the solution, both attain their steady states in a few at units. Now, unless the flux injection from both sides is carefully balanced, $d \approx 0$, after some number of transit times (about $at \approx 10$, say) the current sheet will be 'dominated' by the even solution. The growing gaussian profile near the center (but decreasing as $1/|y|$ on the far away wings) will eventually cancel the sublayer in which the change of sign of the magnetic field (originated from the odd part of the solution) occurs. In the case of exactly balanced flux injection, which corresponds to the presence of an electrostatic field $\mathcal{E}_z$ (constant in space), the presence of an initial even component (a seed magnetic field) may still interfere in the formation of the neutral sublayer. Fig. 6 is obtained by numerical integration in a finite interval (with inflow speed normalized to one) and shows the result of a constant odd magnetic flux injection (with nondimensional values ± 1 at the boundaries, $|y/h_0| = 1$). At $t = 0$ there is also an even seed field in the system ($B/B_0 = 4\cos(\pi y/2h_0)$). One can see the development of the odd driven solution together with the intensification of the even component, so that the asymptotic current sheet becomes asymmetric around $y = 0$, with a reduced neutral sublayer (time is given in units of $1/a$).

Thus, possible scenarios for instabilities or reconnection processes, which one considers on the basis of odd steady state solutions, may not materialize when one examines the formation of the current sheet starting from generic initial conditions.

VIII. Time Evolution of Current Sheets: Applications

As illustrative examples we have chosen different physical regimes: one corresponds to the conditions of the solar atmosphere where prominences are formed, another to fast annihilation of magnetic fields in astrophysical plasmas, and still another to the compressed stage of a plasma focus experiment. It is not our intention to elaborate upon the physics of these complex plasma systems. Our purpose is limited to point out that, if one assumes the presence of a stagnation flow with a magnetic field in the mentioned scenarios, one can get order of magnitude values in ranges adequate to explain fast energy transfer processes.

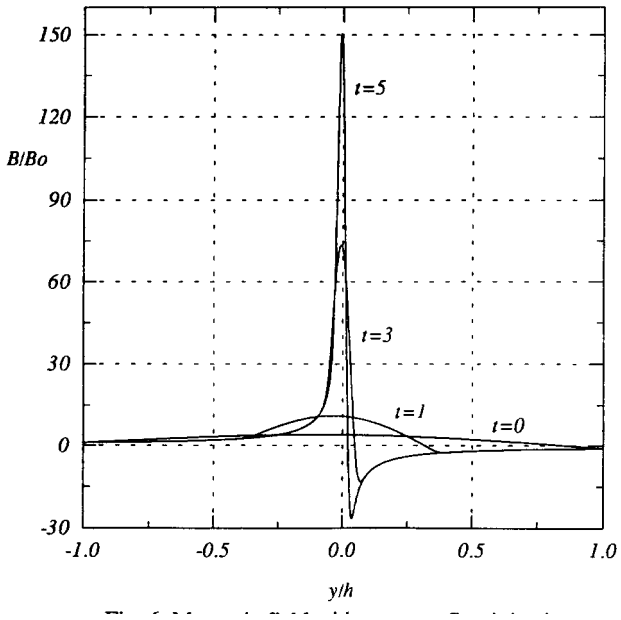

Figure 6. Magnetic field with constant flux injection.

VIII.1 Enhanced dissipation in solar plasmas

Current sheets above the photosphere, particularly in connection with the rising of prominences, have been widely discussed (see, e.g., Refs. [39,25,40]). Let us consider a plasma slab of width $h_o \approx 10^2$ km, the other sides may be much larger $L_x \approx L_z \approx 3000$ km. The slab contains a seed field $B_o \approx 300$ Gauss and the plasma is at about $T = 2 \times 10^5$ °K ≈ 20 ev. The initial magnetic energy in this region is therefore $W_o \approx 3 \times 10^{20}$ Joule. The slab is then squeezed, and we assume a characteristic speed $U_o = 1$ km/sec for the flow (which is much smaller than the sound speed). Since $\nu_m = 10^5 \mathrm{cm}^2/\mathrm{sec}$, we find $R_m = 10^7$, with a rate for the stagnation flow, $a = 10^{-2}$ sec. The energy intensification is about $W \approx \sqrt{R_m} W_o \approx 10^{24}$ Joule. This would be also, approximately, the energy dissipated by joule heating in one *at* unit (i. e., every 100 sec). The time scale for the process is typically $t \approx (1/2a) \ln R_m \approx 800$ sec. These values fit well in order of magnitude with the energy and time of large solar flares. The energy gain per particle in the final resistive layer (in this example $\delta \approx 30$ m) can be very large.

Similar estimates for current sheets in solar physics have been developed by many authors.[40] However, the energy amplification starting from the initial seed is often ommitted (missing a significant $\sqrt{R_m}$ factor). In addition, we note the importance of the stage of formation of the current sheet, in which the odd components are annihilated in free systems, or are dominated by the even components when there is magnetic flux injection (Section VII.2)[18].

VIII.2 Fast annihilation in divergent axial-symmetric flows

Whereas in a planar flow model the result is the dominance of even magnetic components lying in the flow plane, three dimensional diverging flows[18] are characterized by the overall decay of any magnetic seed initially present in the region of interest. As an example of three dimensional flow, we show in Fig. 7 the streamlines for a uniform flow impinging on a spherical interface in a viscous fluid. Fig. 8 shows qualitatively the three dimensional pattern near the stagnation point. Even a constant magnetic flux injection cannot sustain a steady state current sheath near a three dimensional stagnation flow. Steady state structures require a growing flux rate from afar, equivalent to the injection of magnetic energy at a finite rate. Thus, the apparent lack of a large magnetic field intensification at the day side magnetopause, could be explained by the three dimensional nature of the solar wind flow at the magnetosheath. This is the well-known plasma motion that compresses the earth magnetic field, surrounding the magnetospheric obstacle and spreading from the stagnation point in all directions.[47,50,57]

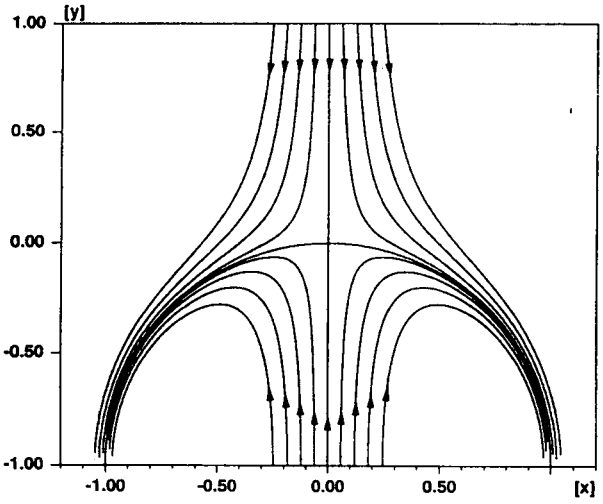

Figure 7. 3-D stagnation point flow at a spherical interface.

Let us consider an axial symmetric flow, y being the symmetry axis, defined by

$$v_x = x\,f', \qquad v_y = -2f, \qquad v_z = z\,f',$$

so that $\mathrm{div}\,\mathbf{v} = 0$. The vorticity is then $\omega = (zf'', 0, -xf'')$, and $\{\mathbf{v}, \omega\} = \mathbf{v}.\mathrm{grad}\,\omega - \omega.\mathrm{grad}\,\mathbf{v} = [2z(f'f'' - ff'''), 0, 2x(f'f'' - ff''')]$, $\mathrm{curl}\,\mathrm{curl}\,\omega = -\nabla^2\omega = (-z\nabla^2 f'', 0, -x\nabla^2 f'')$. Thus, from Eq. (19), and with one integration we find the equation for the flow function f

$$\left(\frac{\partial}{\partial t} - \nu\,\frac{\partial^2}{\partial y^2}\right)\frac{\partial f}{\partial y} = C - \left(\frac{\partial f}{\partial y}\right)^2 + 2f\frac{\partial^2 f}{\partial y^2}, \qquad (120)$$

which has a stagnation point at the origin if we require that $f(0,t)=0$. The constant C measures the pressure gradients in the x,z directions. The magnetic field is assumed of the form $\mathbf{B}=(B_x(y),0,B_z(y))$ so that

$$\mathbf{j}=\frac{c}{4\pi}\left(\frac{\partial B_z}{\partial y},0,-\frac{\partial B_x}{\partial y}\right)$$

and $\{\mathbf{B},\mathbf{j}\}=0$. Writing down Eq. (20) for this case we find

$$\frac{\partial B}{\partial t}=\nu_m\frac{\partial^2 B}{\partial y^2}+2f\frac{\partial B}{\partial y}+f'B\ , \qquad (121)$$

where B stands for B_x or B_z. Clearly, it is possible to combine different initial or asymptotic boundary conditions for B_x and B_z, and build a composite solution for $\mathbf{B}$, with shear of magnetic lines and a different time evolution for each component. We shall only report here the properties of the evolution of one magnetic field component as given by Eq. (121).

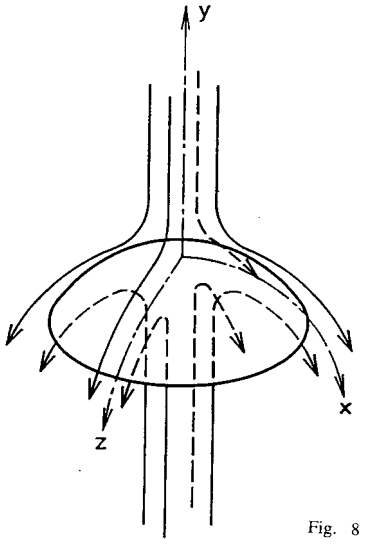

Fig. 8

The pressure field, obtained from the y component of Eq. (2), is given by

$$p = \Pi(y,t)-\frac{1}{2}C(x^2+z^2), \qquad (122)$$

$$\Pi(y,t) = p_0-\left(\frac{B^2}{8\pi}+\frac{1}{2}\rho 2f^2+2\rho\nu f'\right). \qquad (123)$$

We shall assume in the vicinity of the stagnation point a simple, steady state, irrotational flow $f=ay$, where $a=\sqrt{C}$, that satisfies Eq. (120) exactly. Using the transformation of variables

$$\zeta=\frac{y}{h_0}\mathrm{e}^{2at},\ \ \tau=\frac{1}{2R_m}(\mathrm{e}^{2at}-1),\ \ B^*(\zeta,\tau)=h_0\mathrm{e}^{at}B(y,t),$$

we obtain again the classical diffusion equation

$$\frac{\partial B^*}{\partial t}=\frac{\partial^2 B^*}{\partial y^2}, \qquad (124)$$

thus the solutions of the initial value problem of section IV.2 can be used. Multiplying Eq. (121) by $B(y,t)$ and integrating by parts gives

$$\frac{\partial}{\partial t}\int_{-\infty}^{\infty}\frac{B^2}{8\pi}dy=\frac{\nu_m}{4\pi}B\frac{\partial B}{\partial y}\Big]_{-\infty}^{\infty}-\frac{\nu_m}{4\pi}\int_{-\infty}^{\infty}\left(\frac{\partial B}{\partial y}\right)^2 dy. \qquad (125)$$

If $B(y,t)$ goes to zero faster than $1/\sqrt{|y|}$ as $|y|\to\infty$, the total magnetic energy decreases monotonically to zero due to the Joule dissipation. The term that corresponds to magnetic line stretching, aB, is cancelled by the increased advection, $2ay\partial B/\partial y$, represented by the factor 2. Thus, in a three dimensional flow the magnetic field decays asymptotically for $t\to\infty$, and there is no mechanism that can balance diffusion in order to obtain a steady state, as in the case of the B_x component of the planar current sheath model. This result applies even when a constant incoming flux $\lim_{|y|\to\infty} yB$ is being added to the system. For even magnetic fields the decay time can be estimated directly by integration of Eq.(121) assuming $B\to 0$ as $1/|y|^{1+e}$, $e>0$, as $|y|\to\infty$, so that no injection of magnetic flux from infinity occurs,

$$\frac{\partial}{\partial t}\int_{-\infty}^{\infty}B(y,t)dy=-a\int_{-\infty}^{\infty}B(y,t)dy. \qquad (126)$$

Hence assuming $F(t)=\int_{-\infty}^{\infty}B(y,t)dy\neq 0$, we get $F(t)=F_0\exp(-at)$. The decay occurs in a few characteristic times $1/a$.

Detailed descriptions of the decays and the behaviour of the odd solutions can be obtained from self similar solutions, that also exist in this case. Setting, as in Sections VI.1-VI.4, $B=\beta(t)N[\gamma(t)(y-d(t))]$, we find

$$\frac{\dot\beta}{\beta} = a-r\nu_m\gamma^2, \qquad (127)$$

$$\frac{\dot\gamma}{\gamma} = 2a-\nu_m\gamma^2, \qquad (128)$$

$$\dot d = -2a\,d-q\nu_m\gamma, \qquad (129)$$

where r and q are arbitrary constants, and

$$N'' + zN' + (\lambda + 1)N = 0, \qquad (130)$$

where $z = \gamma(t)[y - d(t)] + q$, and $\lambda + 1 = r$. Therefore the parabolic cylinder functions discussed in Sections VI.2-VI.3 are possible similarity solutions in this case also. Magnetic fields that do not diverge in space as $|y| \to \infty$, require that $\lambda > 0$. The temporal behaviour here is different to the planar model. Clearly, the point $\nu_m \gamma^2 \to 2a$ is an attractor for Eq. (128), so that all solutions tend asymptotically to that value, as $t \to \infty$. Therefore, Eq. (127) for the amplitude β, tends asymptotically to

$$\frac{\dot{\beta}}{\beta} \to a[1 - 2(\lambda + 1)]. \qquad (131)$$

Here all self similar solutions with $\lambda \geq 0$ are extinguished. If initially $a >> r\nu_m\gamma_0^2$, which means that $(h_0^2 a/\nu_m) = R_m >> r$, $(\gamma^{-2} \sim h_0)$, after a fast amplification stage with $\beta \sim \exp(at)$ the solutions die as $\beta \sim \exp[-a(1 + 2\lambda)]$. Although the three dimensional flow produces the extinction of the self similar solutions, considerable amplification of the magnetic field and energy dissipation are obtained during the transient when R_m is very large. These effects are illustrated in the following figures. In Fig. 9 we can see the evolution of a Gaussian profile with $\beta/\beta_0 = 1$, $(\gamma_0 h_0/R_m^{1/4}) = 0.1$, and $(d_0/h_0) = 20$, showing the motion towards the origin, the amplification with a maximum ≈ 2.2 at $at \approx 2$ and the extinction with $(\beta/\beta_0) < 0.1$ for $at = 10$. The amplification and extinction of the amplitude $b(t)$ of an elementary solution of the class $(B/B_0) = b(t)\cos[k(t)y]$ with $k_0 = \pi/2$, is shown in Fig. 10 as a function of increasing values of the parameter R_m. The Joule dissipation rate D/aW_0 as a function of at for the same elementary solution, and with R_m as a parameter is shown in Fig. 11. Interestingly, in 3D flows there is no magnetic energy amplification, as can be seen in Fig. 12 which shows the decay of $W(t)/W_0$ as a function of t, for increasing values of R_m. Compare this behavior with the two dimensional flow case where $W(t)/W_0$ is amplified to values larger than 1 before extinction for odd magnetic field solutions.

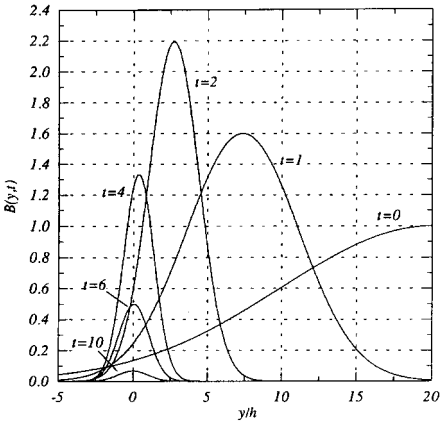

Figure 9. Gaussian self-similar solutions in a 3D flow.

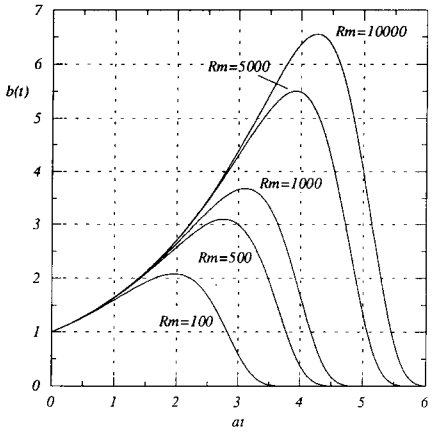

Figure 10. Elementary solution for a 3D flow.

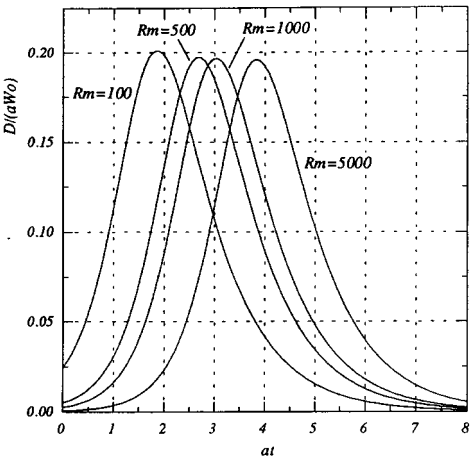

Figure 11. Joule dissipation in a 3D flow.

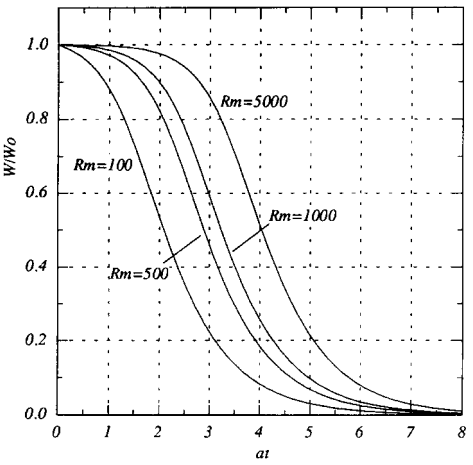

Figure 12. Decay of magnetic energy in a 3D flow.

If there is inflow of magnetic energy in the system, i.e., if the magnetic field decreases as $B \sim 1/\sqrt{|y|}$, for $|y| \to \infty$, so that $|ay|B^2 \to const.$, one can obtain steady state solutions in the three dimensional flow. In the limit of large R_m values one can obtain the solution using a boundary layer approximation. Outside of the current sheet, where the currents are negligible, the magnetic field equation reduces to

$$2y\frac{\partial B}{\partial y} + B = 0, \qquad |y| \to \infty,$$

which is solved by

$$B = \frac{1}{\sqrt{2|y|}}, \qquad |y| \to \infty,$$

and represents the asymptotic behavior for large y. Note that the flux rate $v_y B \sim \sqrt{y}$ diverges at infinity (this is a necesssary condition in view of the previous results). The outer solution must be matched to the resistive layer, which satisfies the equation

$$\frac{\partial^2 B}{\partial r^2} + r\frac{\partial B}{\partial y} + \frac{1}{2}B = 0, \tag{132}$$

where $r = \sqrt{R_m}(y/h)$ with $R_m = 2ah_0^2/\nu_m$. Expressing the magnetic field as

$$B(r) = p(r)e^{-r^2/4}, \tag{133}$$

leads to the equation

$$p'' - \frac{1}{4}r^2 p = 0, \tag{134}$$

which is solved by odd and even parabolic cylinder functions. Matching to the outside solution gives

$$B_{even}(y) = \frac{\Gamma(1/4)}{\sqrt{\pi}} R_m^{1/4} \mathrm{e}^{-\frac{R_m}{2}(\frac{y}{h_0})^2} p_{even}(\sqrt{R_m}y/h_0), \quad 0 < \frac{y}{h_0} < \delta, \tag{135}$$

$$= \frac{1}{\sqrt{2|y/h_0|}}, \qquad \frac{y}{h_0} > \delta, \tag{136}$$

$$B_{odd}(y) = 2\frac{\Gamma(3/4)}{\sqrt{\pi}} R_m^{1/4} \mathrm{e}^{-\frac{R_m}{2}(\frac{y}{h_0})^2} p_{odd}(\sqrt{R_m}y/h_0), \quad 0 < \frac{y}{h_0} < \delta, \tag{137}$$

$$= \frac{1}{\sqrt{2|y/h_0|}}, \qquad \frac{y}{h_0} > \delta, \tag{138}$$

where δ is the width of the current layer ($\delta \sim 1/\sqrt{R_m}$). Both odd and even solutions scale with $R_m^{1/4}$ in spite of the diverging flux rate, and in fact are less intense than in the planar case. Note that the previous analysis is quite general, since any stagnation flow can be approximated locally by $f = ay$ in the vicinity of the stagnation point.

A characteristic scale length for the dayside stagnation point is $h_0 \sim 10^4$ km (bow shock-magnetopause distance), and the magnetosheath plasma velocity is $\sim$ 50 km s^{-1} (near the stagnation point).[44,51] The rate of the stagnation point flow is then $a \sim 5\times10^{-3}$s^{-1}, and the characteristic times for the magnetic field evolution associated with this flow are in the range of 3–10 min-

utes. The magnetic diffusivity ν_m is an unknown and much debated parameter in this region.[21] However, MHD activity with periods ranging from seconds to 10 minutes are constantly perturbing the magnetosheath plasma.[47] In addition, there are major changes in the solar wind pressure and the advected magnetic field with periods of several minutes.[11,23] Thus, it is probable that the steady state current sheaths are never established, and the magnetic field in front of the magnetopause is continuously growing and fading, adjusting to the changes driven by the solar wind. Anyhow, the observed growth of the average magnetic field approaching the magnetopause is at most about a factor 1.5, which would indicate a low value for $R_m \sim 5$, assuming a steady state magnetic field model and the $R_m^{1/4}$ scaling. This would imply a magnetic diffusivity in the 10^{13} cm^2 s^{-1} range, an order of magnitude suggested by several authors for the subsolar magnetosheath.

VIII.3 Plasma Focus.

The plasma focus is an electrical discharge of a capacitor bank between coaxial cylindrical electrodes, open in front like a gun (see Fig. 13). The ionized current sheet (CS) originated at the breach (position (1)) is pushed forward by magnetic forces and after reaching the mouth collapses to the axis of the device where a dense and hot pinch is formed (position (2)). This stage is called a plasma focus (PF).[43] The column of plasma (length: 2–3 cm; diameter: 0.3–0.4 cm) which lasts about 100 ns is an intense source of radiation (x–ray flashes 10–100 keV), particle beams (ions with 1–10 Mev, emitted forwards along the axis, and relativistic electrons, 1 Mev, launched backwards in the inner hollow electrode[33]) and neutrons. These are obtained when the device is filled with deuterium (or a mixture 50 % – 50 % deuterium and tritium) and are produced by the nuclear fusion reactions that take place in the plasma column. These high energy plasma processes are easily produced with fast capacitor banks of 20–80 kJ operating from 20 to 50 kV, with typical periods of 1 μs. Flashes of 10^{10}–10^{11} neutrons of 2.4 Mev from D–D reactions (and 10^{12}–10^{13} neutrons (14 MeV) with tritium operating devices from D–T reactions) with 40 to 80 ns duration, from a point–like source, can be achieved with devices operating at 80 kV, 200 kJ by using several radiation enhancement techniques.[36]

The device is simple and inexpensive to build. Its size (including the vacuum system and the capacitor bank) is moderate and can be transported in a small truck. Technological applications of varied types are being developed now by many national and private laboratories worldwide, exploiting the singular characteristics of this radiation source. The PF is being considered for x–ray lithography of microelectronic components and as a neutron source for a) neutrongraphy, or b) analysis of materials by neutron activation. The tiny size of the source, the almost instantaneous yet intensive flash, and its mobility, makes the device suitable for neutron radiography[34] for the detection of failures or dislocations in metals, particularly when in motion in engines, rotors, turbines, etc. Similarly, transportability and safety of operation makes the PF neutron source adequate for mineral logging or other 'in situ' material analysis by activation, with a clear advantage over the alternative of transporting conventional sources, which are cumbersome and hazardous to manipulate. A PF can be used as a pulsed x-ray source for x-ray lithography with a resolution better that 0.1 μ, avoiding the drawbacks of conventional x-ray sources. We may recall that the increase in spatial resolution is of fundamental importance for microelectronic manufacturing industries.

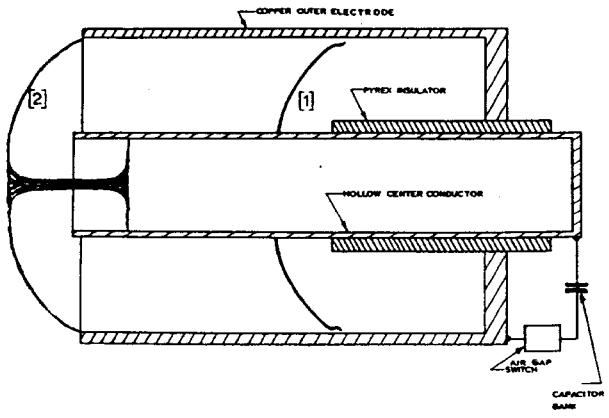

Figure 13. The Plasma Focus.

The plasma focus experiment is a source of high energy ion and electron beams (in the Mev range) as well

as of intense radiation (e. g., x rays) flashes.[5,33] After the formation of the compressed plasma column, very small 'hot spots' (i. e., regions of energy concentration) and highly localized 'neckings' (i. e., strong squeezings) of the pinch, have been observed.[6,9,35] On the other hand, filaments with self-magnetic field, imbedded in the current sheet have been reported both during the coaxial stage of the motion and in the pinched column stage.[4,32] Note also that the focus phase is not an exact cylindrical compression: it shows opening (divergence) along the machine axis. Thus, an outflow along the plasma column takes place.

Let us consider a small plasma slab in the compressed column phase embracing the magnetic field of a filament. For the application of the model we assume initially $h_o = 0.1$ cm (here in a radial direction), $L_x \approx 0.1$ cm (parallel to the axis of the PF), and $L_z \approx 0.1$ cm. The time scales of fine structure events in the records of the emission of particles (including neutrons in deuterium discharges) or x rays are in the order of 10 nsec in PF experiments. We take then $a = 10^8$ sec^{-1} as the rate for a squeezed flow. This corresponds to $|v_y| = h_o a = 10^7$ cm/sec, which is a typical speed for a PF compression. For the plasma temperature in the column we take (initially) $\Theta = 2$ Kev, which gives (using Spitzer's resistivity) $\nu_m = 10^2$ cm^2/sec. Thus, we are dealing with a stagnation flow with $R_m = 10^4$. For the axial filament field we shall assume an initial value $B_o \approx 10^5$ Gauss. During the earlier (more tenuous) coaxial stage, filament fields in the range $3 \times 10^3 - 10^4$ Gauss have been measured, and/or theoretically estimated. It is reasonable to expect higher values in the final pinch, because of the general field intensification by compression. With peak currents of 5×10^5 Amp azimuthal fields near$B_\phi = 10^6$ Gauss can be reached in a PF. Hence we are suggesting 1/10 of this value as representative of filament fields in the compressed stage.

It follows that a dissipative layer of width $\delta \approx 10^{-3}$ cm could be formed with a magnetic energy density $w \approx w_o R_m \approx 4 \times 10^{12}$ erg/cm, in a time lapse of $t_M \approx 40$ nsec. Assuming a plasma density $n \approx 10^{20}$ cm^{-3}, there are about 10^{14} particles in the volume $V_f = 10^{-5}$ cm^3 of a highly localized current layer ($V_f = \delta . L_x . L_z$). Then, in 10 nsec ($at = 1$), the average plasma particle gets a share of $\Theta_f = 2.5$ Mev from the energy dissipated in Joule heating. This estimate is suggestive when correlated with the observed burst of radiation and particles, from several small regions of the plasma column, during the focus stage.

VIII.4 Convergent axial-symmetric flows

These estimates can be supported by a model in cylindrical coordinates that represents better the geometry of plasma focus in the final stage, after the column is formed and a "necking" begins.[15] The equations (31)–(34) can be satisfied exactly by $\xi = (1/2)ar^2 z$ and $\psi = \psi(r,t)$ so that we have the following velocity and magnetic field,

$$v_z = az \quad , \quad v_r = -\frac{1}{2}ar \quad (v_\phi = 0 \; ; a = \text{constant}) \tag{139}$$

$$B_z = B_z(r,t) \; , \quad B_\phi = B_\phi(r,t) \quad (B_r = 0) \; . \tag{140}$$

Equations (33)–(34) reduces then to the following

$$\frac{\partial B_z}{\partial t} = \nu_m \frac{1}{r}\frac{\partial}{\partial r}(r\frac{\partial B_z}{\partial r}) + \frac{a}{2}\frac{1}{r}\frac{\partial}{\partial r}(r^2 B_z), \tag{141}$$

$$\frac{\partial (rB_\phi)}{\partial t} = \nu_m \frac{\partial}{\partial r}(\frac{1}{r}\frac{\partial (rB_\phi)}{\partial r}) + \frac{ar^2}{2}\frac{\partial}{\partial r}(\frac{rB_\phi}{r^2}) \; . \tag{142}$$

It is easy to verify that these equations are also valid if the Hall term is taken into account. In fact (see Appendix)

$$[\psi, \frac{1}{r^2}\mathcal{D}^2\psi] = [\frac{h_\phi^2}{2}, \frac{1}{r^2}] = [h_\phi, \psi] = 0,$$

with the assumption that ψ and h_ϕ depends on r, t only. It is also not difficult to verify that a may also be a function of time and satisfy $\dot{a} = C - a^2$, the same equation of the planar irrotational motions (see Section III.3). Here C is related to the pressure gradient along z: $(\partial p/\partial z) = -Cz$.

The change of B_z in time can be studied by self–similar solutions of the type

$$B_z = b(t) H[s\frac{R_m}{2}\gamma(t)(\frac{r}{r_0})^2] \; , \tag{143}$$

where s is an arbitrary real number, $R_m \equiv r_0^2 a/2\nu_m$, r_0 a typical radial scale for the initial axial magnetic field,

$B_z(t=0)$. $H(z)$ is a function of the self–similar variable $z = (s/2)R_m\gamma(t)(r/r_0)^2$, to be determined. The time–varying amplitude $b(t)$, and the changing spatial scale factor $\gamma(t)$ in Eq.(143) satisfy the following equations

$$\frac{\mathrm{d}\gamma}{\mathrm{d}t} = a\gamma(1-\gamma)\ , \tag{144}$$

$$\frac{\mathrm{d}b}{\mathrm{d}t} = ab[1-(\lambda+1)\gamma] \tag{145}$$

where λ is an arbitrary real number. Then $H(z)$ is any solution of the ordinary differential equation

$$zH'' + (1+z)H' + (\lambda+1)H = 0\ . \tag{146}$$

Solutions with regular behaviour for $r = 0$ are given by $H(z) = \exp(-z)M(-\lambda, 1, z)$, M being Kummer's function (confluent hypergeometric). When $\lambda = n$ is a positive integer we have $M(-n,1,z)/n! = L_n(z)$, the Laguerre polynomial of order n. Thus we can choose

$$H(z) = n!\ \mathrm{e}^{-z}L_n(z) \tag{147}$$

and in view of the linearity of Eq. (141) we can add any set of these self–similar solutions to obtain the solution of the initial value problem for a given B_z at $t = 0$. The radial scale factor and the amplitude are given by

$$\gamma = \frac{\gamma_0}{\gamma_0 + (1-\gamma_0)e^{-at}}\ , \tag{148}$$

$$b = \frac{b_0 e^{-nat}}{[\gamma_0 + (1-\gamma_0)e^{-at}]^{n+1}}\ . \tag{149}$$

The important case $n = 0$ gives the evolution of a Gaussian magnetic field ($s = 1$)

$$B_z = \frac{b_0 \exp[-\frac{R_m}{2}\gamma(t)(\frac{r}{r_0})^2]}{\gamma_0 + (1-\gamma_0)\exp(-at)}\ . \tag{150}$$

Taking $\gamma_0 = 1/R_m << 1$, the field is concentrated in a thin Gaussian filament of radius $\delta \approx r_0 R_m^{-1/2}$, since $\gamma(\infty) = 1$ as $t \to \infty$. The field amplitude is intensified from b_0 at $t = 0$ to $b_0 R_m$ for $t \to \infty$. The asymptotic state is approached in a short lapse of order $\tau \approx (1/2)\ln R_m$ (i. e., in a few hydrodynamic periods $1/a$). While the plasma motion continues, the filament strongly dissipates energy as shown by

$$D = \frac{\pi}{16}R_m^2\left(\nu_m \frac{b_0^2}{8\pi}\right)\ , \tag{151}$$

the asymptotic rate for Joule heating per unit length.

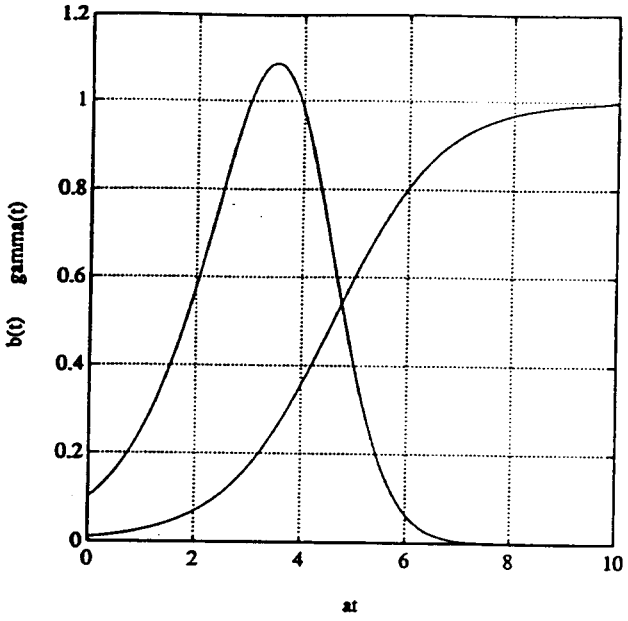

Figure 14. Self similar solutions for n=3 (radially convergent flow).

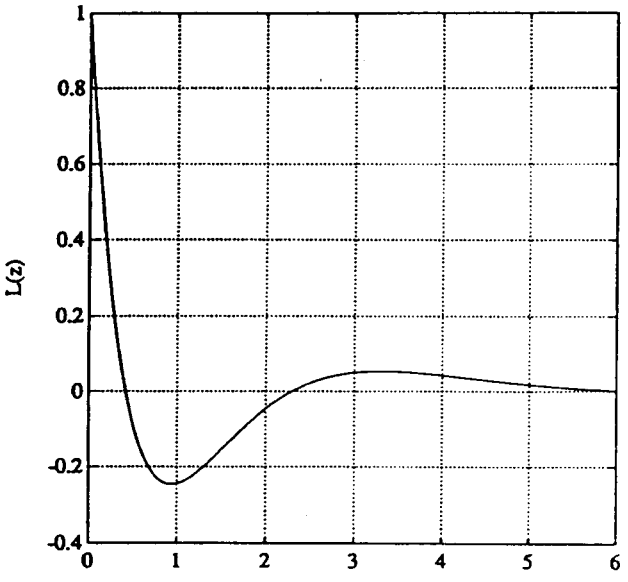

Figure 15. Laguerre function for n=3.

For all $n \geq 1$, Eq. (149) shows that the field first grows (if $\gamma_0 < 1$) and then extinguishes completely. The reason being that Eq. (141) conserves the total magnetic flux $F = \int \pi B_z d(r^2)$, which is zero for Eq. (147) profiles with $n \geq 1$. As time goes by, positive and negative fluxes are pushed together by the flow, and

annihilate each other. The energy dissipated by these components may also be considerable. As an example, Figs. 14 and 15 show the time evolution and shape of the self–similar solution for $n = 3$.

VIII.5 Collapse of a magnetic field filament and particle acceleration

In the secondary pinching driven by the B_ϕ component we can take in order of magnitude $b_0 \approx 10^5$ Gauss, $a \approx 10^8$ s^{-1}, $r_0 \approx 0.1$ cm, $T_e \approx 2$ keV, so that $\nu_m \approx 10^2$ cm^2 /s and $R_m \approx 10^4$. We find, assuming the plasma density in the range $n \approx 10^{20}$ cm^{-3} and a length $\Delta z \approx 0.1$ cm, a Joule heating equivalent to 30 keV per particle and per nanosecond, over a small volume $\approx 10^{-6}$ cm^{-3} with $\approx 3 \times 10^{-3}$ cm in radius. These values are consistent with the previous estimates (Section VIII.3) based on the planar current sheath model (we discuss the particle heating further in Section X). The B_z magnetic field may grow up to ≈ 200 MGauss. These values can be correlated with the appearance of hot spots in the hard X rays imaging of the plasma column,[5,9] the neutron emission in deuterium discharges and with fields in the 10^8 MGauss range reported in the literature.[4,6,32,35]

It can be shown that the dissipation generated by the B_ϕ component is negligible compared with that originated by B_z, the reason being that there is no stretching of field lines for this component. The maximum for B_ϕ in the collapse stage of the Plasma Focus is in the 10^8 Gauss range, because experimental values for $B_0 = 2I/cr_0$ are in the MGauss order, thus convalidating the assumption that the B_ϕ component is the driver for the process of intensification and dissipation of the axial component B_z.[32,35]

The column of plasma that suffers the necking with axial outflow will last only a short time period until the collapse is completed. Indicating with $r = \zeta(t)$ the radial position of the column free boundary we have

$$\frac{\mathrm{d}\zeta}{\mathrm{d}t} = v_r]_{r=\zeta} = -\frac{1}{2}a\zeta.$$

Hence if a is a constant $\zeta = r_0 \exp[-(1/2)at]$ and the collapse to the axis takes place in a few times $1/a$. If the necking of the column starts at $t = 0$, when a constant value $C = C_0$ is established, with $a(t = 0) = 0$, then from $\dot{a} = C_0 - a^2$, we obtain $a = a_0 \tanh(a_0 t)$, $a_0 = \sqrt{C_0}$, and for the motion of the boundary $\zeta = r_0/(\cosh(a_0 t))^{1/2}$ which approaches asymptotically to the previous result. However, it is plausible that the secondary pinching produces a pressure gradient that grows with $B_\phi^2/8\pi$ as in an $m = 0$ pinch instability. Therefore, $C(t) \sim C_0(r_0/\zeta)^2$ taking $B_\phi \sim 2I/c\zeta$ at the boundary. Note also that the axial outflow of the pinched plasma column prevents the stabilization of the $m = 0$ mode due to the presence of the axial field B_z. With this assumption for $C(t)$ we can write

$$\dot{a} = C_0 \left(\frac{r_0}{\zeta}\right) - a^2,$$
$$\dot{\zeta} = -\frac{1}{2}a\zeta,$$

with $\zeta = r_0$, and $a = 0$ at $t = 0$. Thus, setting $z = (\zeta/r_0) \leq 1$ and $\tau = a_0 t$ $(a_0 = \sqrt{C_0})$ we have

$$z'' = -\left(\frac{1}{2} + 3z'^2\right)\frac{1}{z}, \quad z = 1, z' = 0, \quad \text{at } \tau = 0,$$

denoting with z' the derivative with respect to τ. This is a motion with unbounded aeleration as $z \to 0$. The collapse takes place on a much shorter scale than $1/a_0$ (see Fig. 16). The amplification of B_z is intensified, but more important at higher speed, so that the induced electric fields become very large. When the necking of the column is completed the axial current is interrupted. The fast decay of B_ϕ generates an E_z electric field oriented to restabilize the axial current. From Faraday's induction law $E_z \sim (1/c)(B_\phi/\Delta t)r_0$ where Δt is the time scale of the collapse. Thus, the accelerating potential can be estimated as

$$\phi(Volt) \sim \frac{B_0 r_0 l}{\Delta t} \times 10^{-8} \qquad (152)$$

where l is the acceleration length. Taking $B_\phi \sim 10^7 - 10^8$ Gauss, $r_0 \sim l \sim 0.1$ cm., and $\Delta t \leq 1$ ns,[9] assuming $\Delta t \sim (1/10)(1/a)$ we obtain values of ϕ in the

Megavolt range. Note that the electrons are accelerated toward the gun while the ions in the z axis direction, according to the observed relativistic electrons[33] and Mev ion beams. Thus, in addition to the heating that may be achieved through the intensification of the B_z component, a fast disruption of the plasma column at the necking may explain the origin of the high energy particles. This estimate is based on the intensification of B_ϕ and the collapse speed. In Ref. 9 the lifetime of the hot spots is estimated in the ns range.

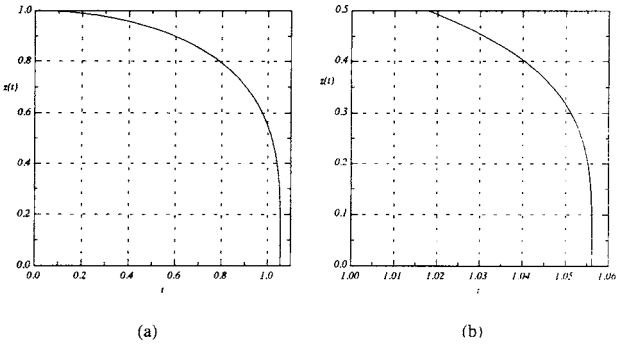

Figure 16. Collapse of the plasma column in the PF.

IX. Comments on the Stability of the Dissipative Layers

A question that may arise is whether the dissipative structures that we are studying are stable. We have shown that the overall picture that emerges from the analysis of the time evolution of the current layers is quite different from that of an equilibrium, or a steady state current sheath, with antiparallel magnetic field lines. The balanced magnetic flux injection of magnetic fields with opposite sign is the exception, rather than the rule. We have often used a magnetic field with constant signature as the basic element for a strongly dissipative layer. We have seen also that the evolution of the magnetic fields takes place on the fast hydrodynamic scale, and that the odd solutions fade, when there is no injection for these components, or they are dominated by the even magnetic field when generic magnetic flux injection occurs. In three dimensional stagnation point flows, the fast extinction of magnetic fields is a common case. Therefore, we should distinguish between specific steady state (or equilibrium) current sheath configurations, where the concepts of reconnection or tearing modes have been intensively studied, and the more general class of time dependent current layers that we have considered. When a strong even magnetic filament develops, like the Gaussian solutions we have encountered, the system tends to be MHD stable, and the tearing concept, of course, does not apply. On the other hand, if there also exists an important B_ϕ component, like in the case of the plasma focus model, then we have a pinch magnetic field configuration modified by the presence of the flow. The radial converging flow we have analyzed is Section VIII, aims to model an instability: the 'necking' or secondary pinching observed in the plasma column of the device.

In the special case of a driven current sheath with an odd magnetic field profile, tearing and reconnection of magnetic lines may be envisaged. To begin with the tearing instability: a theory of the tearing modes for a current layer with a zero order stagnation point flow does not exist yet for the B_x component, i.e., for the field amplified by line stretching (Section IV). This is due to the theoretical difficulties of the intrinsically two dimensional perturbation problem (for a partial attempt in the WKB approximation, see [8]). For the steady state B_z component of Section IV (that is only advected by the flow, see Fig. 2), the problem of the tearing modes can be reduced to one dimension by Fourier analysis[38] (like in the classical treatment of resistive instabilities in an equilibrium current sheath,[14]). The results of the stability analysis are shown in Figs. 17a,b. The perturbations are of the form $\exp(\lambda t + ik_z z)$, and the growth rate λ and wavelength k_z are expressed in nondimensional form $p = \lambda/a$, $k = k_z\sqrt{\nu_m/a}$, respectively.

In Fig. 17a, p is shown as a function of k, for a magnetic Prandtl number $P_m = \nu/\nu_m = 10^{-5}$, with the Lundquist number, $S = V_A/\sqrt{a\nu_m}$ (where the scale length $h = \sqrt{\nu_m/a}$), as a varying parameter. The stabilization effect of the convection rate a on the tearing

instability of a driven current sheath can be noted: as a increases, S diminishes (the scale length of the current layer decreases) until p becomes negative for all k values (for $S \lesssim 10$).

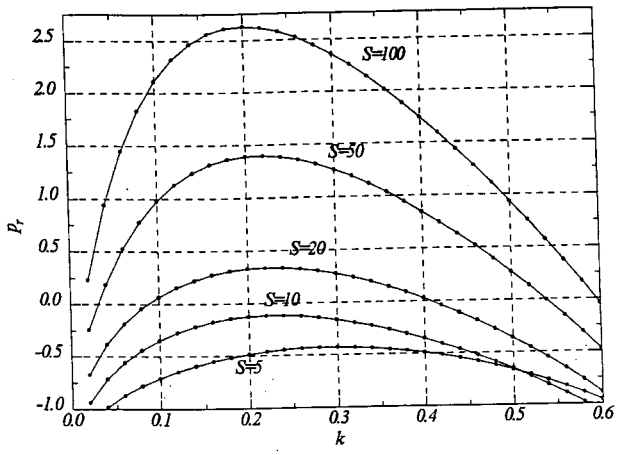

Figure 17a. Growth rates for the tearing mode (constant viscosity).

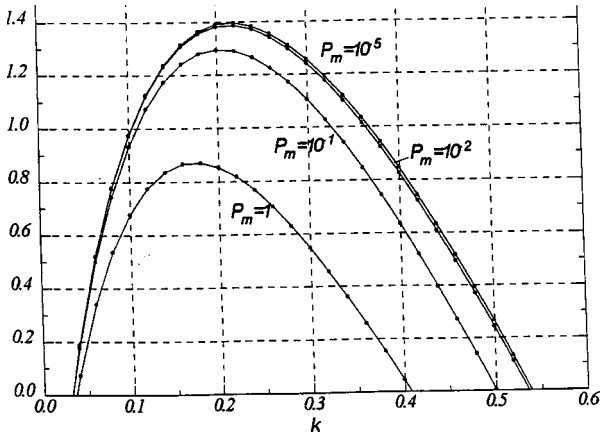

Figure 17b. Effect of viscosity on the tearing mode (S=50).

In Fig. 17b we can see the influence of viscosity in moderating the growth rate of the tearing modes. Here $S = 50$ is fixed and the viscosity changes so that the magnetic Prandtl number varies in the interval $10^{-5} \leq P_m \leq 1$. The stabilizing influence of viscosity is well known. In [22] it is shown that the growth rate for tearing modes of an equilibrium current sheath is not a function of S and P_m separately, but rather a function of $S/P_m^{1/2} = H_a$, the Hartmann number. The scaling is $p = \lambda h^2/\nu_m \propto H_a^{1/3}$ (h is the current layer width) which indicates a stabilizing influence with increasing viscosity. It is also noted in [22] that the growth rate scales with the temperature as $\lambda \propto T^{-5/3}$. The viscosity influence, then, may be important in solar physics current layers, where the temperature increases by a factor 10^2 from the chromosphere to the corona.

We cannot apply the stability results for B_z to the B_x component. However, there are indications that the current layer for B_x may be even more stable than that associated with B_z. There are theoretical reasons and numerical computations pointing in that direction. The perturbative equations for tearing modes of a B_x^0 configuration driven by an irrotational flow $\xi^0 = axy$ are given in [22]. Denoting with $B_{1y}(x, y, t)$ the y component of the perturbative magnetic field (i.e., the reconnection component, normal to the zero order B_x^0 field) and with $\xi_1 = \xi_1(x, y, t)$ the perturbation of the stream function, it is found that

$$\frac{\partial}{\partial t}\int \frac{B_{1y}^2}{8\pi} dS = -\nu_m \int |\mathrm{grad}\, B_{1y}|^2 dS - \int \frac{B_x^0}{4\pi} B_{1y} \frac{\partial^2 \xi_1}{\partial x^2} dS - a\int dS, \tag{153}$$

where $dS = \mathrm{d}x\mathrm{d}y$. The first two rhs terms are typical of the tearing mode energy balance for an equilibrium current sheath. The first produces the decay of B_{1y}^2 by Joule dissipation, the second is the possible cause of growth of the tearing instability. The third one is due to the zero order flow. Clearly it represents a stabilizing term (absent in the case of the B_z component) due to the (negative) stretching term $B_{1y}\partial v_y^0/\partial y$. In other words, while the flow amplifies B_x components it reduces B_y components (unstretching), acting, therefore, against the tearing instability.

Qualitatively this argument applies also to a recon-

nection component B_y. When the $\xi = axy$ flow advects a B_y component from afar, B_y decreases along the trajectory. The effect opposes the permanence of a reconnected configuration. In fact, the numerical simulations performed by several authors[2,27,60] show precisely this effect. Starting from a reconnected field pattern, as time proceeds, the current layer tends to consolidate while the reconnection component fades. In Figs. 18a,b MHD numerical solutions (L. Bender, 1993) with $R_m = U_0 h/\nu_m = 100$ and $M_A = U_0\sqrt{4\pi\rho}/B_0^2 = 1$ show the consolidation of the current sheet from $tv_0/h = 0.5$ to $tv_0/h = 1.5$. Biskamp[2,3] argues against the Petsheck reconnection model, in view of the fact that in the numerical solutions the current sheet length tends to grow and to approach a Sweet-Parker scaling. Tearing islands appear only for large aspect ratios. In [27], which presents a compressible MHD numerical simulation, the current sheet also tends to consolidate. The authors speak of intermittent (or "bursty") reconnection that occurs for long current sheaths. Ref. [60] also shows the consolidation of the current sheath against reconnection in simulations with uniform resistivity. Reconnection is induced "ad-hoc" in [60] by assuming anomalously large resistivity values in the neighborhood of the origin (non uniform resistivity).

Finally, let us show the relationship and differences of the build-up scaling corresponding to the models of the present paper, and the Sweet-Parker[54,37] scaling. The Sweet-Parker concept is usually presented for reconnection processes, although as a limit case it contains also the dissipation of magnetic flux in a non reconnected current layer (annihilation of magnetic field). The basic idea is shown in Fig. 19a where the inflow carries a magnetic field B_i, with velocity v_i towards the current sheath (of thickness δ^* and length L). Reconnection is assumed to be the driver of the motion, with a reconnected magnetic field B_o in the outflow. The continuity equation gives $v_i/v_0 \sim \delta^*/L$ (v_0: outflow velocity). The pressure at the inflow is nearly equal to the outflow pressure. Thus, Bernouilli's equation

$$p_i + \frac{B_i^2}{8\pi} + \frac{1}{2}\rho v_i^2 = p_c = p_0 + \frac{B_0^2}{8\pi} + \frac{1}{2}\rho v_0^2$$

(p_c is the pressure at the stagnation point, where $B = 0$, $v = 0$) gives $v_0^2 \sim B_i^2/(4\pi\rho) = V_{Ai}^2$ (since $(B_0/B_i)^2 \ll 1$ and $(v_i/v_0)^2 \ll 1$). In a steady state, the incoming magnetic flux is balanced by dissipation in the current sheath, so that $v_i \sim v_D \sim \nu_m/\delta^*$. From these equations we get $(\delta^*/L) = 1/\sqrt{S_i} = v_i/V_{Ai} = M_{Ai}$, where $S_i = LV_{Ai}/\nu_m$, is the inflow Lundquist number. The inflow Alfvenic Mach number measures the reconnection speed, i.e. the rate at which the incoming flux is processed through the current layer.

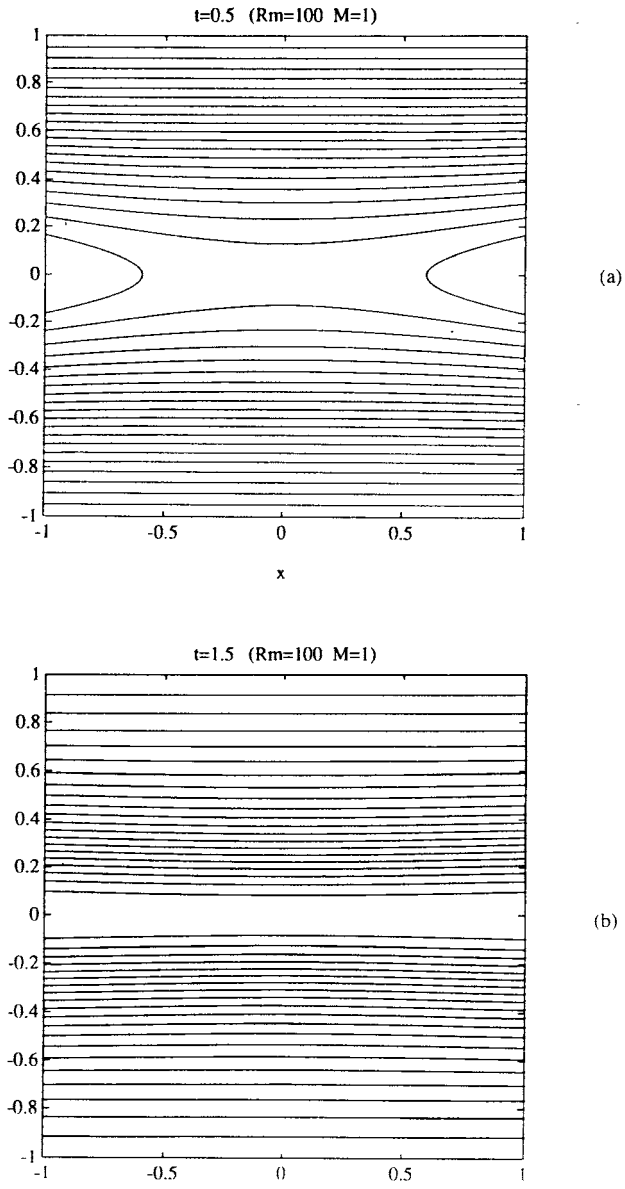

Figure 18. Consolidation of the current sheet.

The scaling in the build-up models of Section IV is different from the Sweet-Parker scaling because of

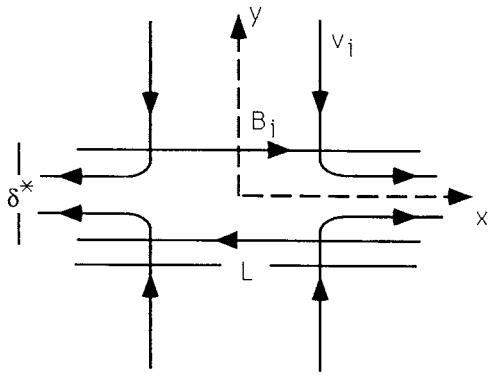

Fig. 18 (a). Sweet-Parker scaling.

Figure 19(a). Sweet-Parker scaling.

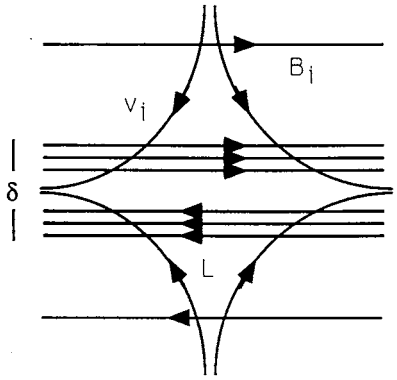

Fig. 18 (b). Pile-up scaling.

Fig. 19(b). Pile-up scaling.

the magnetic field intensification at the current sheath, and the presence of an external driver. In the build-up model following the y and x axis through the center (see Fig. 18b) we have $v_i \sim v_0$ at the same distance from the stagnation point. We know, from Section III , that $\delta/L \sim 1/\sqrt{R_m}$, taking $h \sim L$ and $R_m \sim v_i L/\nu_m$. In addition, the field is intensified at $y \sim \delta$ to the value $B_M \sim \sqrt{R_m} B_i$. The incoming flux $v_i B_i$ is balanced by dissipation at the rate $v_i B_i \sim (\nu_m B_M)/\delta$. Therefore, $v_i/V_{Ai} = M_{Ai}$ is not restricted to a particular value, and may be arbitrarily large, depending on the available external force. Furthermore, since $R_m = M_{Ai} S_i$, then $\delta/\delta^* = 1/\sqrt{M_{Ai}}$.

X. Thermal Effects and Compressibility: an Outline

X.1 Thermal enhancement of the current sheath build-up

The MHD equations, including a temperature dependence of the magnetic diffusivity $\nu_m(T)$, thermal conductivity $\lambda(T)$, and kinematic viscosity $\nu(T)$, for a flow with $\operatorname{div} \mathbf{v} = 0$ can be written as

$$\frac{\partial \mathbf{v}}{\partial t} + \omega \times \mathbf{v} = -\operatorname{grad}\left(\frac{p}{\rho} + \frac{v^2}{2}\right) + \frac{\operatorname{curl} \mathbf{B} \times \mathbf{B}}{4\pi\rho} + \operatorname{div}\left(2\nu \operatorname{grad} \mathbf{v}\right), \tag{154}$$

$$\frac{\partial \mathbf{B}}{\partial t} - \operatorname{curl}\left(\mathbf{v} \times \mathbf{B}\right) = \operatorname{div}\left(\nu_m \operatorname{grad} \mathbf{B}\right), \tag{155}$$

$$\left(\frac{\partial}{\partial t} + \mathbf{v} \cdot \operatorname{grad}\right) 3\, nkT = \operatorname{div}\left(\lambda \operatorname{grad} T\right) + \frac{\nu_m}{4\pi} (\operatorname{curl} \mathbf{B})^2, \tag{156}$$

where n is the (constant) number density ($\rho = nm$, k: Boltzmann's constant). In Eq. (156) we ignore the additional heat source $2\rho\nu(\operatorname{grad} \mathbf{v})^2$ generated by viscous dissipation, assuming that the Joule heating is the dominant effect. In a plasma the growth of T reduces the magnetic diffusivity, and the effective value of R_m increases. Thus, an enhancement of the dissipative effects at the current sheet is expected. Under certain conditions, the model may be prone to a thermal runaway[16]. To this purpose the dependence of resistivity with temperature and magnetic field, as they are predicted by plasma transport theory, are included. We have

$$\nu_m = \nu_{mo} \left(\frac{T}{T_0}\right)^{-3/2}$$

for the magnetic diffusivity, and

$$\lambda = \lambda_{\|0}\frac{T^{5/2}}{1+(\frac{\lambda_{\|0}}{\lambda_{\perp 0}})(\frac{B}{B_0})^2(\frac{T}{T_0})^3}$$

for the thermal conductivity. It can be verified that the MHD equations are exactly satisfied by the following velocity, magnetic field and temperature assumptions: a) Planar: $v_x = ax$, $v_y = -ay$, $B_x = B(y,t)$, $T = T(y,t)$ ($v_z = B_y = B_z = 0$); b) Cylindrical: $v_z = 2az$, $v_r = -ar$, $B_z = B(r,t)$, $T = T(r,t)$ ($v_\phi = B_r = B_\phi = 0$). The magnetic field evolution is coupled to the temperature equation as follows

$$\frac{\partial B}{\partial t} = \frac{1}{\zeta^s}\frac{\partial}{\partial \zeta}\left(\nu_{mo}(\frac{T}{T_0})^{-3/2}\zeta^s\frac{\partial B}{\partial \zeta}\right) + a\zeta\frac{\partial B}{\partial \zeta} + (s+1)aB, \quad (157)$$

$$3n\frac{\partial (kT)}{\partial t} = \frac{1}{\zeta^s}\frac{\partial}{\partial \zeta}\left(\lambda_{\|0}\frac{(T/T_0)^{5/2}}{1+(\lambda_{\|0}/\lambda_{\perp 0})(B/B_0)^2(T/T_0)^3}\zeta^s\frac{\partial (kT)}{\partial \zeta}\right)$$
$$+3na\zeta\frac{\partial (kT)}{\partial \zeta} + \frac{\nu_{mo}}{4\pi}(\frac{T}{T_0})^{-3/2}(\frac{\partial B}{\partial \zeta})^2, \quad (158)$$

where s=0 corresponds to planar flow ($\zeta = y$) and s=1 to the cylindrical case ($\zeta = r$). We use here the classical $T^{3/2}$ dependence of the electrical conductivity, where T_0 is the initial (uniform) plasma temperature. The thermal conductivity is across the field lines since $\partial T/\partial x = 0$ in this model ($\partial T/\partial z = 0$ for s=1). The perpendicular conductivity $\lambda_{\perp 0}$ used corresponds to the values given by Braginskii in the strong field limit[7]; $\lambda_{\|0}$ is the isotropic conductivity ($B = 0$). The term with $(\partial B/\partial y)^2$ in the temperature equation represents the Joule heating due to the magnetic field dissipation and acts as a driver of T changes, so that $T = T_0$ is not a solution. The system is ruled now by a pair of nonlinearly coupled equations of diffusion-reaction type, including advection and amplification effects. Equations (157) and (158) can be solved numerically using an implicit finite difference scheme of second order on a non uniform grid that concentrates points in the dissipative layer. The discrete equations are solved iteratively at each time step using nonlinear multigrid method and a correction procedure which allows the use of a relatively coarse convergence criterion for the iteration process.[24] The calculations are carried out until a steady state is reached or until the numerical grid can no longer resolve the narrow current layer developed as a consequence of the thermal runaway.

X.2 Non dimensional parameters and their influence

The initial-value problem is solved in the interval $-h \le y \le h$ in which the magnetic field at $t = 0$ is assigned. If there is no injection of magnetic flux (which could be carried in by the flow) h is the scale length of the initial magnetic seed, that is amplified by the motion as time goes by. On the other hand, if there is continuous injection of magnetic flux (transported from distant plasma regions) the boundary value of the magnetic flux rate will fix the h scale (equivalently: the inflow speed $U = ah$, and the magnetic field B_0 at $y = h$).

The non dimensional parameters that govern the solutions are: the magnetic Reynolds number $R_m = ah^2/\nu_{mo}$, the Péclet number $P_e = ah^2/\kappa_0$ (with $\kappa_0 = \lambda_{\|0}/3n_0$, the isotropic thermal diffusivity), the ratio of of the isotropic and perpendicular conductivities $\gamma = (\lambda_{\|0}/\lambda_{\perp 0})$, and $\epsilon = ({B_0}^2/8\pi)/(3n_0kT_0)$ equal to the ratio of initial magnetic and thermal energies. The thickness of the current sheet and the magnetic field amplification (by line stretching) depend on R_m. Only for $R_m \gg 1$ large values of Joule heating can be achieved. Thermal losses by diffusion in the outer wings of the current layer (where $B \approx 0$) are related to P_e. The temperature growth in the current sheet depends on γ (more precisely on $P_e\gamma$). When this number is small, thermal losses by diffusion are important and the

current layer may not heat up significantly. Finally, the thermal blow up depends on the energy initially available for conversion into heat via the energy ratio ϵ. If $\epsilon \gg 1$, when $R_m \gg 1$, $P_e \gg 1$, the solutions easily run away. Conversely, the threshold for a significant temperature growth is found at small values of these parameters.

Other important factors that influence the thermal evolution are the parity of the magnetic fields (odd, even) and the magnetic flux injection. In absence of flux injection the runaway effect is more difficult to produce, since the system then relies only on the initial magnetic seed.

X.3 Joule dissipation and blow-up

These features are illustrated with solution examples in Figs. 20–23, where the total Joule heating (per unit area and unit time) $D(t) = (\nu_{mo}/4\pi) \int_{-h}^{h} (T/T_0)^{-3/2} (\partial B/\partial y)^2 dy$ in a planar ($s = 0$) current sheet (measured in units of aW_0; $W_0 = (1/8\pi) \int_{-h}^{h} B_0^2 dy$ the total initial magnetic energy per unit area) is given as a function of at. In Figs. 20 to 22 the magnetic field is even, $B(t=0) = B_0 \cos(\pi y/2h)$, and there is no flux injection. The influence of ϵ is shown in Fig. 20 ($R_m = 1000$, $P_e = 0.01$, $\gamma = 100$). When $\epsilon = 0$ (reference case without thermal effects (Eq. (157) with $T = T_0 = constant$, studied in Section IV), the field reaches a dissipative steady state (a thin Gaussian profile) in which amplification and dissipation are balanced. The ongoing dissipation of this remnant field feeds the temperature equation. Then, we see that passing from $\epsilon = 0.01$ to $\epsilon = 1$ the runaway develops over a short time scale. The influence of γ and R_m is shown in Fig. 21 ($R_m = 1000$, $P_e = 0.01$, $\epsilon = 0.1$) and Fig. 22 ($P_e = 0.01$, $\gamma = 100$, $\epsilon = 0.1$), respectively. In all these examples we can see that large values of the parameters lead to runaway solutions. In Fig. 23, the influence of R_m is studied in the case of an odd magnetic field $B(t=0) = B_0 \sin(\pi y/2h)$ with no flux injection. The solid lines correspond to $\epsilon = 0.1$ ($P_e = 0.01$, $\gamma = 100$) and the dashed lines represent constant temperature solutions with $\epsilon = 0$. In this example the magnetic field is completly annihilated after an amplification stage. The thermal coupling enhances the dissipation but no runaway occurs.

In Section VIII we have shown the relevance of flow enhanced energy dissipation (at a stagnation point) for plasmas in the physical conditions of the solar atmosphere and the Plasma Focus device (origin of hot spots). Let us examine whether the energy dissipation may not become more intense due to a thermal runaway process.

As an example for solar applications we take physical parameters adequate for the transition region from chromosphere to corona: $T = 20$ eV, $n = 10^9$ cm^{-3}, and assume $B_0 = 300$ Gauss, $h = 10^7$ cm, $U = 10^5$ cm/s for the initial current sheet and inflow speed. Very large values of the non dimensional parameters characterize this case: $R_m = 1.1 \times 10^7$, $P_e = 8.6 \times 10^{-3}$, $\gamma = 1.3 \times 10^{13}$, and $\epsilon = 3.7 \times 10^4$. These large values prevent a direct use of the numerical program because of grid size problems. But, from experience gained from smaller values and the physics of the model, there is no doubt that a thermal runaway occurs. In such plasma conditions we expect that even at moderate speeds a stagnation flow leads to a large localized energy deposition. If turbulent motions are induced in this plasma regime, the random collisions of eddies will generate here and there local squeezings (transient stagnations points) and then a chaotic series of fast energy releases (microbursts) may appear.

As in Section VIII consider a 'necking' (secondary pinching) of the plasma column (cylindrical geometry, s=1) for the application of the stagnation flow model to the Plasma Focus experiment. The following physical conditions are assumed for this example: $T = 2000$ eV, $n = 10^{20}$ cm^{-3}, $B_0 = 10^5$ Gauss, $h = 0.1$ cm and $U = 10^7$ cm s^{-1}. We obtain $R_m = 1.1 \times 10^4$, $P_e = 8.3 \times 10^{-3}$, $\gamma = 150$, and $\epsilon = 4.2 \times 10^{-4}$. For these values the thermal runaway develops very quickly due to the higher efficiency for energy dissipation of a radially convergent flow, as can be seen in Fig. 24.

X.4 Heating and Compressibility limits

Using non dimensional variables, $y \to y/h$, $B \to B/B_0$, $T \to T/T_0$, $t \to at$, we can write for a planar flow (keeping the same notation for simplicity)

$$\frac{\partial B}{\partial t} = \frac{1}{R_m}\frac{\partial}{\partial y}\left(\hat{\nu}_m(T)\frac{\partial B}{\partial y}\right) + y\frac{\partial B}{\partial y} + B, \tag{159}$$

$$\frac{\partial \Delta T}{\partial t} = \frac{1}{P_e}\frac{\partial}{\partial y}\left(\hat{\lambda}(T,B)\frac{\partial \Delta T}{\partial y}\right) + y\frac{\partial \Delta T}{\partial y} + \frac{\epsilon}{R_m}\hat{\nu}_m(T)\left(\frac{\partial B}{\partial y}\right)^2. \tag{160}$$

We have set $\Delta T = T - 1$, so that $\Delta T \to 0$, as $|y| \to \infty$. Here $\hat{\nu}_m(T) = \nu_m/\nu_{m0}$, $\hat{\lambda}(T,B) = \lambda_\perp(T,B)/\lambda_{\perp 0}$.

In the case of liquid metals a similar equation holds but λ, being isotropic, is function of the temperature only, and $\epsilon = (B_0^2/4\pi)/\rho_0 C T_0$ contains the specific heat C per unit mass of the material. The temperature dependence of the transport coefficients in liquid metals is quite different from that of plasmas. Often, in preliminary studies it is ignored, assuming constant values for $\hat{\nu}$, $\hat{\lambda}$. In plasmas $\epsilon \sim 1/\beta$, so that the incompressible approximation that we are using implies values of ϵ smaller than one. The source of Joule heat in Eq. (160) seems to be weak for this case, particularly in comparison with the advective cooling term $y\partial\Delta T/\partial y$, which brings cold material to the current sheath continuously from afar. However, we must keep in mind that it is for large R_m values that the Joule heating becomes important, and in fact $(1/R_m)(\partial B/\partial y)^2$ becomes a large number in the chosen units.

We can discuss these matters with energy balances derived from Eqs. (159)–(160), by integration. Asuming $|y\Delta T| \to 0$ as $|y| \to \infty$ we find from Eq. (160)

$$\frac{\partial}{\partial t}\Delta E = -\Delta E + 4\pi\epsilon D, \tag{161}$$

and integrating Eq. (159) after multiplication by $B/4\pi$,

$$\frac{\partial}{\partial t} W = -D + W. \tag{162}$$

Here we have defined

$$\Delta E \equiv \int_{-\infty}^{\infty} \Delta T dy, \quad W \equiv \int_{-\infty}^{\infty} \frac{B^2}{8\pi} dy, \quad D \equiv \frac{1}{4\pi R_m}\int_{-\infty}^{\infty} \hat{\nu}_m(T)\left(\frac{\partial B}{\partial y}\right)^2 dy.$$

When the plasma is limited in y, as in the case of the plasma focus column, the integration range extends only to the plasma-vacuum boundary. At this boundary $\partial\Delta T/\partial y = 0$, since heat conduction is null there. At $t = 0$, $\Delta T = 0$, and $\partial\Delta E/\partial t = 4\pi\epsilon D > 0$, so that ΔE begins to grow. Ordinarily $D \sim O(1)$ in the initial stage, so that the growth rate depends on ϵ. As soon as $\Delta E \sim O(1)$ the cooling term in Eq. (161) becomes important. Combining Eqs.(161)–(162), we get $\partial(\Delta E + 4\pi\epsilon W)/\partial t = 4\pi\epsilon W - \Delta E$. Thus the total energy, internal and magnetic, grows only when $4\pi\epsilon W > \Delta E$. A steady state is posible, in principle, when asymptotically $D \to W$, and simultaneously $4\pi\epsilon W \to \Delta E$. We have shown (Sections III–IV) that (in non dimensional units) the energy amplification in the planar case is $W \sim \sqrt{R_m}$. Thus, assuming a steady state case $\Delta E \sim 4\pi\epsilon\sqrt{R_m}$. We can see that the increase in internal energy depends on the product $\epsilon\sqrt{R_m}$, and may attain large values even if $\epsilon << 1$, provided that $4\pi\epsilon\sqrt{R_m} >> 1$.

The equations (161)-(162) can be derived also in the case of the cylindrical flows; the only change is in

the definitions of the integrals. For instance $\Delta E = \int \Delta T 2\pi r dr$, and similarly for D and W. Therefore, the conclusions can be extended also to the cylindrical flow model, remembering that the amplification is larger, $W \sim R_m$, so that $\Delta E \sim 4\pi\epsilon R_m$ if a steady state has been achieved. On the other hand, if in the intensification stage of the current sheath, when $D \sim W$, it happens that $4\pi\epsilon R_m > \Delta E$, then a thermal runaway occurs. The discussion suggests that $4\pi\epsilon R_m^{s/2} > 1$ ($s = 1$: planar flow; $s = 2$: cylindrical flow) is the condition for the thermal enhancement effect and that above this limit a thermal runaway may occur.

If the intensification process takes place in a high beta plasma region (for instance, a place with a small magnetic field seed) $\beta_0 = 10$ say, and $R_m = 10^4$, $\epsilon \sim 1/\beta_0$ we have $4\pi\epsilon R_m^{1/2} \sim 120$ and the thermal enhancement process would start. At the beginning the incompressible model is within the validity limit. As the field is amplified the change of the plasma beta is $\beta/\beta_0 \sim T/B^2$ and roughly $\beta/\beta_0 \sim \Delta E/W \sim 4\pi\epsilon \sim 1$. Therefore, the evolution may take place most of the time within the validity limit of the incompressible model. The increase in the magnetic field is accompanied by a temperature growth, that moderates the descent of β. Conversely, in a region of low β, $\epsilon \sim 1/\beta_0 >> 1$, and if R_m is small, say $R_m \sim O(1)$, the amplification effect is negligible, so that the magnetic field changes will not affect the plasma density. However, the heating effect is very important, $4\pi\epsilon W > \Delta E$, and the plasma β will grow locally.

Of course, there are ranges of R_m and ϵ values such that the incompressible model breaks down during the build-up, when changes ΔB^2 in the magnetic pressure produce significant variations of density. Very little is known about these regimes, and the important problem of the limits of the amplification process and the thermal effects is still open. The extension of the research to compressible plasmas certainly requires a major computational physics effort. In most cases the fast extinction processes presented in previous sections are not affected by these remarks. The first stage of the amplification process is, in general, also within the limits of the incompressible approximation, when the driven motion is subsonic. But in low beta plasmas, or for very large R_m values, or both, the incompressibility condition cannot last very long. The limitation is that $(1/\rho)(\mathrm{d}\rho/\mathrm{d}t)$ must be a small number along the trajectory of the plasma elements, and this is no longer true when the pressure suffers large changes due to the magnetic field evolution. The theory presented here, although suggestive that important magnetic and thermal effects are to be expected, must be superseded by a full scale compressible calculation. This is not yet available for the processes analyzed here, but research has been started on compressibility effects in reconnection problems.[40,55,42,13,46,27,26,60]

These comments do not apply to the case of conducting liquids: extinction and amplification of magnetic fields always occur with $\mathrm{div}\,\mathbf{v} \approx 0$. Let us examine the case of a) liquid sodium in large systems for breeding or fusion reactors, and b) the molten metals of the earth's liquid core (see Table I). For large scale industrial applications R_m may reach a few times 10 at most, $C \sim 4 \times 10^6$ erg/g K and at $T_0 = 373$ K, $\epsilon \sim 0.04$ assuming a field of 5000 Gauss.[29,31] Therefore amplification and heating by the process envisaged here are not significant. The case of the Earth's core is different, since R_m values in the range from 10^3 to 10^5 seem possible.[61,30] Thus, fast amplification or extinction, by line stretching, may happen. The inner poloidal field is modest, in the 10 Gauss range at most, while the (unobservable) toroidal component is estimated to be a few times 10^3 Gauss. Taking $\rho \sim 10$ g cm^{-3}, $C \sim 0.1$ cal/g K and $T \sim 5000$ K, we get $\epsilon \sim 10^{-6}$ for the toroidal component. Therefore, although interesting amplification effects are possible, the heating effects are insignificant. These comments do not imply that in liquid metals thermal processes are not important. In fact, boundary conditions (hot walls) or high frequency electromagnetic fields, or buoyancy forces (local thermal expansion), may certainly produce important effects.[30,31] We have not, however, considered these topics here.

XI. Conclusions.

Convection and stretching of magnetic field lines by plasma motions with a stagnation point can account for a large amplification, or a fast extintion rate, of

magnetic fields over the hydrodynamic time scale. The analysis of the time evolution of current sheaths driven by plasma motions shows that the configurations commonly considered as models for steady state reconnection or for tearing instability studies, are exceptional cases rather than generic magnetic structures. Regarding magnetic components lying in the plane of the motion, a two-dimensional stagnation flow tends to privilege even solutions during the formation of the current sheet: a) in a system without magnetic flux injection because it is the only part that survives after a transient, and b) in flux driven solutions because the even part increases without bounds linearly with time while the odd part tends to a steady state. In nature, unbalanced configurations of magnetic fluxes are probably the rule, and the cases with injected flux $\phi \approx 0$ exceptions, since the fluxes that enter from both sides of a squeezed plasma are ordinarily not tailored.

On the other hand, the magnetic component normal to the plane of the motion is ordinarily extinguished, except under special conditions of magnetic flux injection. The behaviour of current layers in three dimensional stagnation flows is quite different from that of similar planar flow models. All magnetic fields not sustained by a permanent magnetic energy injection from afar suffer a fast decay. Applications of the initial value problem for the formation of current sheaths has been given in several fields: solar physics, space physics, and plasma focus experiments.

The mechanism of flow enhanced dissipation may be further intensified by thermal efects for some plasma conditions. Solar plasmas are very sensitive to this process in view of the large values of R_m, P_e and ϵ. Losses due to radiation, or gradients along the current sheet, not included in our calculations may become relevant in particular systems. An important effect to be considered in the next step of the research is the density variation (plasma depletion) that may occur during the current sheet evolution, under conditions of large magnetic field amplification.

Acknowledgments

Research supported by CONICET PID-BID grant N° 0594–92, Dynamics of Plasmas and Fluids, and INFIP-CONICET, and also in part by grant UBA EX092. F.T.G. and G.G. are members of CONICET and Professors at UBA, G.G. is Associate Member of the International Centre for Theoretical Physics, Trieste, Italy. L.B. is a CONICET Research Fellow.

Appendices

Appendix 1. Orthogonal Curvilinear Coordinates.

To the representation Eqs.(22)–(23) we may add another divergenceless field in the following way. Let (α, β, γ) stand for an arbitrary curvilinear coordinate set, $X^1 = \alpha$, $X^2 = \beta$, $X^3 = \gamma$, with $\mathbf{e}_i = \partial \mathbf{x}/\partial x^i$,$\mathbf{e}^i = \operatorname{grad} x^i$, the covariant and contravariant vector bases respectively ($\mathbf{x}$denotes here the position vector). We shall write $|d\mathbf{x}|^2 g_{ij} dx^i dx^j$ for the determinant of g_{ij}, following standard notations. Then $w\mathbf{e}^i/\sqrt{g}$, is a solenoidal vector field, with field lines aligned with the coordinate x^i, provided that the function $w(x^k)$ does not depend on x^i. From now on, we shall specify the ignorable coordinate with γ, we may write then, instead of Eqs. (22)–(23),

$$\mathbf{v} = \operatorname{grad}\xi \times \operatorname{grad}\zeta + \frac{1}{\sqrt{g}} w \mathbf{e}_\gamma, \qquad (163)$$

where $w = w(\alpha, \beta)$, for a vector field with $\operatorname{div}\mathbf{v} = 0$, and similarly for $\mathbf{h}$. Note that the last term is of the form $w\operatorname{grad}\alpha \times \operatorname{grad}\beta$, which may be rewritten as $\operatorname{grad}\alpha \times \operatorname{grad}\zeta'(\alpha, \beta)$, where $\zeta' = \int^\beta w(\alpha, \beta')d\beta'$, so that it is essentially a special case of Eq. (22).

The reduction of the MHD equations was obtained in [20]. We give here the final formulas because of the wide spectrum of problems that can be treated using them. Using the basic representations that follows, the interested reader can derive the results as an exercise.

When the coordinates are orthogonal the reduced equations simplify considerably. The metric will be written as $ds^2 = (l_\alpha d\alpha)^2 + (l_\beta d\beta)^2 + (l_\gamma d\gamma)^2$, where l_α, l_β, l_γ are the Lamé scale factors and $\sqrt{g} = l_\alpha l_\beta l_\gamma$. The γ coordinate must be ignorable in the metric factors also. In the following expressions $\xi = \xi(\alpha, \beta)$, $\psi = \psi(\alpha, \beta)$, and $v_\gamma(\alpha, \beta)$, $h_\gamma(\alpha, \beta)$, are the covariant components of $\mathbf{v}$ and $\mathbf{h}$. The operator $\mathcal{D}^2$ is the γ covariant component

of $-(\mathrm{curl}\,\mathrm{curl}\,)_\gamma$, as in $(\mathrm{curl}\,\mathrm{curl}\,\mathbf{v})_\gamma = -\mathcal{D}^2 v_\gamma$. Starting from

$$\mathbf{a} = \mathrm{grad}\,A \times \mathbf{e}^\gamma + \frac{1}{l_\gamma^2}\psi \mathbf{e}^\gamma, \tag{164}$$

it is not difficult to compute

$$\mathbf{h} = \mathrm{grad}\,\psi \times \mathbf{e}^\gamma + \frac{1}{l_\gamma^2} h_\gamma \mathbf{e}_\gamma, \tag{165}$$

$$\mathbf{v} = \mathrm{grad}\,\xi \times \mathbf{e}^\gamma + \frac{1}{l_\gamma^2} v_\gamma \mathbf{e}_\gamma, \tag{166}$$

$$\mathbf{J} = \mathrm{grad}\,h_\gamma \times \mathbf{e}^\gamma + \frac{1}{l_\gamma^2}\mathcal{D}^2\psi \mathbf{e}_\gamma, \tag{167}$$

$$h_\gamma = -\mathcal{D}^2 A, \tag{168}$$

$$\mathrm{curl}\,\mathrm{curl}\,\mathbf{h} = -\mathrm{grad}\,\mathcal{D}^2\psi \times \mathbf{e}^\gamma - \frac{1}{l_\gamma^2} h_\gamma \mathbf{e}_\gamma, \tag{169}$$

$$\mathrm{curl}\,\mathrm{curl}\,\mathbf{v} = \mathrm{grad}\,\mathcal{D}^2\xi \times \mathbf{e}^\gamma - \frac{1}{l_\gamma^2} v_\gamma \mathbf{e}_\gamma, \tag{170}$$

$$\mathrm{curl}\,\mathrm{curl}\,\omega = -\mathrm{grad}\,\mathcal{D}^2 v_\gamma \times \mathbf{e}^\gamma - + \frac{1}{l_\gamma^2}\mathcal{D}^2\mathcal{D}^2\xi \mathbf{e}_\gamma, \tag{171}$$

From which one can obtain

$$\mathbf{J} \times \mathbf{h} = -\left(\frac{1}{\sqrt{g}}[\psi, h_\gamma]\mathbf{e}^\gamma + \frac{1}{l_\gamma^2}\mathcal{D}^2\psi\,\mathrm{grad}\,\psi + \frac{1}{l_\gamma^2} h_\gamma \mathrm{grad}\,h_\gamma\right), \tag{172}$$

$$\{\mathbf{h}, \mathbf{J}\} = \mathrm{grad}\left(\frac{1}{\sqrt{g}}[h_\gamma, \psi]\right) \times \mathbf{e}^\gamma - \frac{1}{\sqrt{g}}\left([\frac{1}{l_\gamma^2}\mathcal{D}^2\psi, \psi] + [\frac{1}{l_\gamma^2}, \frac{h_\gamma^2}{2}]\right)\mathbf{e}_\gamma, \tag{173}$$

and similar formulas for $\omega \times \mathbf{v}$, $\{\mathbf{v}, \omega\}$. Here we have introduced the bracket

$$[f, g] = \frac{\partial(f, g)}{\partial(\alpha, \beta)} = \frac{\partial f}{\partial \alpha}\frac{\partial g}{\partial \beta} - \frac{\partial f}{\partial \beta}\frac{\partial g}{\partial \alpha},$$

as a shorthand notation for the Jacobian of the functions f, g with respect to the variables α, β. Thus we have all the elements needed for the equations (14), (15), (19), and (20). Note that

$$\mathrm{grad}\,\xi = \frac{\partial \xi}{\partial \alpha}\mathbf{e}^\alpha + \frac{\partial \xi}{\partial \beta}\mathbf{e}^\beta,$$

and therefore

$$v^\alpha = \frac{1}{\sqrt{g}}\frac{\partial \xi}{\partial \beta}, \qquad v^\beta = -\frac{1}{\sqrt{g}}\frac{\partial \xi}{\partial \alpha},$$

and a similar representation for h^α, h^β. The physical components are given by

$$v_{<i>} = h_{(i)} v^i = \frac{1}{h_{(i)}} v_i, \quad \text{for } i = \alpha, \beta, \gamma,$$

so that

$$v_{<\alpha>} = \frac{1}{l_\beta l_\gamma}\frac{\partial \xi}{\partial \beta}, \quad v_{<\beta>} = \frac{1}{l_\alpha l_\gamma}\frac{\partial \xi}{\partial \alpha}, \quad v_{<\gamma>} = \frac{v_\gamma}{l_\gamma},$$

$$h_{<\alpha>} = \frac{1}{l_\beta l_\gamma}\frac{\partial \psi}{\partial \beta}, \quad h_{<\beta>} = \frac{1}{l_\alpha l_\gamma}\frac{\partial \psi}{\partial \alpha}, \quad h_{<\gamma>} = \frac{h_\gamma}{l_\gamma}.$$

Appendix 2. The reduced MHD equations.

For the flow on the α, β plane and the motion normal to it we obtain for the stream function ξ and the covariant v_γ component the following equations

$$\frac{1}{l_\gamma^2}\mathcal{D}^2\left(\frac{\partial \xi}{\partial t} - \nu\,\mathcal{D}^2\xi\right) = \frac{1}{\sqrt{g}}\left([\frac{1}{l_\gamma^2}\mathcal{D}^2\psi, \psi] + [\frac{1}{l_\gamma^2}, \frac{h_\gamma^2}{2}]\right) \tag{174}$$

$$- \frac{1}{\sqrt{g}}\left([\frac{1}{l_\gamma^2}\mathcal{D}^2\xi, \xi] - [\frac{1}{l_\gamma^2}, \frac{v_\gamma^2}{2}]\right) \tag{175}$$

$$\frac{\partial v_\gamma}{\partial t} - \nu\,\mathcal{D}^2 v_\gamma = \frac{1}{\sqrt{g}}\left([h_\gamma, \psi] - [v_\gamma, \xi]\right), \tag{176}$$

with

$$\mathcal{D}^2 = \frac{l_\gamma}{l_\alpha l_\beta}\left[\frac{\partial}{\partial\alpha}\frac{l_\beta}{l_\alpha l_\gamma}\frac{\partial}{\partial\alpha} + \frac{\partial}{\partial\beta}\frac{l_\alpha}{l_\beta l_\gamma}\frac{\partial}{\partial\beta}\right]. \tag{177}$$

The operator $\mathcal{D}^2$, denoted also by Δ^* in the literature on plasma equilibria, was introduced by Stokes for cylindrical and spherical coordinates in his classical hydrodynamical works.[28]

For the magnetic field the equations reduce to

$$\left(\frac{\partial}{\partial t} - \nu_m\,\mathcal{D}^2\right)\psi = \frac{1}{\sqrt{g}}[\xi, \psi] - \frac{1}{k}\frac{1}{\sqrt{g}}[h_\gamma, \psi], \tag{178}$$

$$\frac{1}{l_\gamma^2}\left(\frac{\partial}{\partial t} - \nu_m\,\mathcal{D}^2\right)h_\gamma = \frac{1}{\sqrt{g}}\left([\xi, \frac{h_\gamma}{l_\gamma^2}] - [\psi, \frac{v_\gamma}{l_\gamma^2}]\right)$$

$$- \frac{1}{k}\frac{1}{\sqrt{g}}\left([\psi, \frac{1}{l_\gamma^2}\mathcal{D}^2\psi] + [\frac{1}{2}h_\gamma^2, \frac{1}{l_\gamma^2}]\right). \tag{179}$$

The projection of the momentum equation, Eq. (14), on the plane α, β is

$$\text{grad}\left(\frac{\partial}{\partial t} - \nu\,\mathcal{D}^2\right)\xi \times \mathbf{e}^\gamma = \text{grad}\,P + \frac{1}{l_\gamma^2}\left(\mathcal{D}^2\xi\text{grad}\,\xi + \text{grad}\,\frac{v_\gamma^2}{2}\right)$$

$$- \frac{1}{l_\gamma^2}\left(\mathcal{D}^2\psi\text{grad}\,\psi + \text{grad}\,\frac{h_\gamma^2}{2}\right) \tag{180}$$

from which the pressure can be obtained as an exact diferential taking the scalar product with $\delta\mathbf{x} = d\alpha\mathbf{e}_\alpha + d\beta\mathbf{e}_\beta$. If we introduce the operator δ^* by

$$\delta^* \stackrel{def}{=} (\delta \times \text{grad}\,)\,.\mathbf{e}^\gamma = \frac{l_\alpha}{l_\beta l_\gamma}\text{d}\alpha\frac{\partial}{\partial\beta} - \frac{l_\beta}{l_\alpha l_\gamma}\text{d}\beta\frac{\partial}{\partial\alpha}$$

Taking the scalar product with $\delta\mathbf{x}$ we get the exact differential

$$dPdP = -\delta^*\left(\frac{\partial}{\partial t} - \nu\,\mathcal{D}^2\right)\xi + \frac{1}{l_\gamma^2}\left(\mathcal{D}^2\xi\text{d}\xi + \text{d}\frac{v_\gamma^2}{2}\right)$$

$$- \frac{1}{l_\gamma^2}\left(\mathcal{D}^2\psi\text{d}\psi + \text{d}\frac{h_\gamma^2}{2}\right) \tag{181}$$

from which the pressure distribution, Eq. (7) may be computed.

References

1. D. Biskamp. *Magnetic Reconnection Lecture Notes*, Lecture Notes of the 1993 Spring College in Plasma Physics , ICTP, Trieste, Italy, May-June 1993.
2. D. Biskamp. Magnetic reconnection via current sheets, Phys. Fluids, **29**, 1520 (1986).
3. D. Biskamp, *Nonlinear Magnetohydrodynamics*, Cambridge University Press, 1994.
4. W. H. Bostick, V. Nardi, and W. Prior. Similarities between solar flares and laboratory hot plasma phenomena. In K. Schindler ed., editor, *Cosmic Plasma Physics*, pages 175–184, Plenum, New York, 1971.
5. W. H. Bostick, V. Nardi, and W. Prior, X-ray fine structure of dense plasmas in a co-axial accelerator, J. Plasma Phys., **8**, 7 (1972).
6. W. F. Bostick et al. Megagauss fields and current patterns in focused discharges. In A. Turchi, editor, *Megagauss Physics and Technology*, page 533, Plenum, New York, 1980.
7. S. I. Braginskii. *Transport Processes in a Plasma*, chapter , pages 205–311. Volume 1 of *Reviews of Plasma Physics*, Consultants Bureau, New York, 1965.
8. S. V. Bulanov, J. Sakai. and S. I. Syrovatskii. Tearing mode instability in approximately steady MHD configurations. Sov. J. Plasma Phys., **5**, 157 (1979).
9. P. Choi, R. Aliaga-Rossel, C. Dumitrescu-Zoita, and C. Deeney. Dynamics of hot spots formation in a dense plasma focus optical and x-ray observation. In, *Proc. 3rd Int. Conf. on Dense Z-Pinches*, London, 1993.
10. A. Clark Jr. Production and dissipation of magnetic energy from differential fluid motions. Phys. Fluids, **7**, 1299 (1964).
11. C. J. Farrugia, M. P. Freeman, S. W. H. Cowley, and D. J. Southwood. Plasma-driven magnetopause motions and attendant response on the ground. Planet. Space Sci., **37**, 589 (1989).
12. T. G. Forbes and E. R. Priest. A comparison of analytical and numerical models for steadily driven magnetic reconnection. Rev. Geophys., **25**, 1587 (1987).
13. T. G. Forbes, E. R. Priest, and A. W. Hood. Evolution of current sheets following the onset of enhanced resistivity. J. Plasma Phys., **27**, 157 (1982).
14. H. P. Furth, J. Killeen, and M. N. Rosenbluth. Finite resistivity instabilities in a sheet pinch. Phys. Fluids, **6**, 459 (1963).
15. F. T. Gratton and L. Bender. Fast energy dissipation in an axial symmetric mhd flow. In M. F. Heyn, W. Kernbichler, and H. K. Biernat, editors, *Proc. Int. Workshop Plasma Physics, Pichl bei Schladming*, Graz University Press, 1993.
16. F. T. Gratton and L. Bender. Thermal blow-up of current sheets. In M. F. Heyn, W. Kernbichler, and H. K. Biernat, editors, *Proc. Int. Workshop Plasma Physics, Pichl bei Schladming*, Graz University Press, 1993.
17. F. T. Gratton, L. Bender, and G. Gnavi. Fast dissipation of magnetic fields by plasma motions. In H. K. Biernat, G. Bachmaier, S. J. Bauer, and R. P. Rijnbeek, editors, *The Solar Wind–Magnetosphere System, Proceedings of the International Workshop held in Graz, Austria, September 23–25, 1992*, pages 335–342, Austrian Academy of Sciences Press, Vienna, 1994.
18. F. T. Gratton, G. Gnavi, and L. Bender. Development of strongly dissipative mhd structures. *IEEE Trans. Plasma Science, Special Issue on Cosmic and Space Plasma*, **20(6)**, 882 (1992).
19. F. T. Gratton, G. Gnavi, M. F. Heyn, H. K. Biernat, and R. P. Rijnbeek. Pressure drive and viscous dragging: a reply. J. Geophys. Res., **95**, 261 (1990).
20. F. T. Gratton and M. F. Heyn. *The Reduced Equations of Dissipative Incompressible Magnetohydrodynamics and Some of Their Exact Integrals.* Technical Report IWF8903, Institut für Weltraumforschung, Graz, 1989.
21. F. T. Gratton, M. F. Heyn, H. K. Biernat, R. P. Rijnbeek, and G. Gnavi. Mhd stagnation point flows in the presence of resistivity and viscosity. J. Geophys. Res., **93**, 7318 (1988).

22. F. T. Gratton and R. Krasnopolsky. Stability of current sheets: finite-dimensional approximations to the spectrum. In H. K. Biernat, G. Bachmaier, S. J. Bauer, and R. P. Rijnbeek, editors, *The Solar Wind Magnetosphere System, Proceedings of the International Workshop held in Graz, Austria, September 23–25, 1992*, pages 343–357. Austrian Academy of Sciences Press, Vienna, 1994.
23. F. T. Gratton, C. J. Farrugia, and S. W. H. Cowley. Is the magnetopause Rayleigh-Taylor unstable sometimes? J. Geophys. Res., **101**, 4929 (1996).
24. A. Hirt and A. Harlow. J. Comput. Phys., **19**, 163 (1967).
25. M. Jardine. Magnetic reconnection in solar flares, Chapter 9. In E. R. Priest and A. W. Wood editors, *Advances in solar system magnetohydrodynamics*, Cambridge University Press, Cambridge, 1991.
26. M. Jardine and E.R. Priest. Energetics of compressible models of fast steady-state reconnection. J. Plasma Phys., **43**, 141 (1990).
27. S.-P. Jin and W.-H. Ip. Two-dimensional compressible magnetohydrodynamic simulation of the driven reconnection process. Phys. Fluids B, **3(8)**, 1927 (1991).
28. H. Lamb. *Hydrodynamics.* Cambridge University Press, 6th. edition, 1957.
29. J. Lielpeteris and R. Moreau (Eds.). *Liquid Metal Magnetohydrodynamics.* Kluwer, Dordrecht, The Netherlands, 1989.
30. H. K. Moffat. *Magnetic field generation in electrically conducting fluids.* Cambridge University Press, London, 1978.
31. R. Moreau. *Magnetohydrodynamics.* Kluwer, Dordrecht, The Netherlands, 1990.
32. V. Nardi, W. H. Bostick, and W. Prior. Magnetic fields higher than 100 MG produced in the current sheath of a co-axial accelerator. In *Physique sous Champs Magnetiques Intenses, Colloques Internationaux, Vol. 242*, pages 129–138, CNRS, France, 1973.
33. V. Nardi, W. H. Bostick, J. Feugeas, and W. Prior. Internal structure of electron-beam filaments. Physical Rev. A, **22**, 2211 (1980).
34. V. Nardi and J. S. Brzosko. *Neutron Radiography Workshop, Los Alamos 1987.* LANL-11393-C Suppl. UC414, Los Alamos Natl. Lab., Jan. 1989.
35. V. Nardi et al. Megagauss fields and current patterns in focused discharges. In C. W. Fowler et al., editor, *Proc. IV Conf. on Magnetic Field Generation Santa Fe, New Mexico, U.S.A., July 1986*, pages 269–277, Plenum, New York, 1987.
36. V. Nardi et al. Stimulated acceleration and confinement of deuterons in focused discharges, Part i and ii. IEEE Trans. Plasma Sci., **16(3)**, 368 (1988).
37. E. N. Parker. *Spontaneous Current Sheets in Magnetic Fields.* Oxford University Press, 1994. See, also, The solar flare phenomenon and the theory of reconnection and annihilation of magnetic fields. Astrophys. J. Suppl. Ser., **8**, 177 (1963).
38. T. D. Phan and B. U. Ö. Sonnerup. Resistive tearing-mode instability in a current sheet with equilibrium viscous stagnation-point flow. J. Plasma Phys., **46**, 407 (1991).
39. E. R. Priest. Current sheets, Chapter 3. In *Solar Flare MHD*, Gordon and Breach, London, 1981.
40. E. R. Priest. The mhd of current sheets. Rev. Prog. Phys., **48(7)**, 995 (1985).
41. E. R. Priest and T. G. Forbes. New models for a fast steady state magnetic reconnection. J. Geophys. Res., **91**, 5579 (1986).
42. E. R. Priest and L. C. Lee. Nonlinear magnetic reconnection models with separatrix jets. J. Plasma Phys., **44**, 337 (1990).
43. J. P. Rager. The plasma focus. In *Unconventional Approaches to Fusion*, B. Brunelli and G. Leotta editors, pages 157–193, Plenum, New York, 1982.
44. R. P. Rijnbeek, H. K. Biernat, M. F. Heyn, V. S. Semenov, C. J. Farrugia, D. J. Southwood, G. Paschmann, N. Sckopka, and C. T. Russell. The structure of the reconnection layer observed by ISEE 1 on 8 september 1978. Annales Geophysicae, **7**, 297 (1989).
45. P. H. Roberts. *An Introduction to Magnetohydrodynamics.* Longmans, 1967.

46. T. Sato, T. Hayashi, K. Watanabe, R. Horiuchi, M. Tanaka, N. Sawairi, and K. Kusano. Role of compressibility on driven magnetic reconnection. Phys. Fluids B, **4(2)**, 450 (1992).
47. M. Saunders. The earth's magnetosphere, Chapter 16. In *Advances in solar system magnetohydrodynamics*, E. R. Priest and A. W. Wood, editors, Cambridge University Press, 1991.
48. B. F. Shutz. *Geometrical Methods of Mathematical Physics*. Cambridge University Press, Cambridge, 1980.
49. B. U. Ö Sonnerup. Magnetic field reconnection. In *Solar System Plasma Physics, Vol.III*, L. T. Lanzerotti et al. eds., pages 47–108, North Holland, 1979.
50. B. U. Ö. Sonnerup. Magnetic field reconnection in a highly conducting incompressible fluid. J. Plasma Phys., **4**, 161 (1970).
51. B. U. Ö. Sonnerup, G. Paschmann, I. Papamastorakis, N. Sckopka, G. H. Haerendel, S. J. Bacne, J. R. Asbridge, J. J. Gosling, and C. T. Russell. Evidence for magnetic field reconnection at the earth's magnetopause. J. Geophys. Res., **86**, 10049 (1981).
52. B. U. Ö. Sonnerup and E. R. Priest. Resistive mhd stagnation-point flows at a current sheet. J. Plasma Phys., **14(2)**, 283 (1975).
53. D. P. Stern. Amer. J. Phys., **38**, 494 (1970).
54. P. A. Sweet. The production of high energy particles in solar flares. Nuovo Cimento Suppl. Ser. X, **8**, 188 (1958).
55. T. Tajima. *Computational Magnetohydrodynamics, Chapter 14*. Benjamin, 1991.
56. L. Turner. IEEE Trans. Plasma Sci., **14**, 849 (1986).
57. V. M. Vasyliunas. Theoretical models of magnetic field merging. Rev. Geophys. Space Phys., **13**, 303 (1975).
58. R. B. White. Rev. Mod. Phys., **58**, 183 (1986).
59. R. B. White. Resistive instabilities and field line reconnection. In M. N. Rosenbluth and R. Z. Sagdeev, editors, *Handbok of Plasma Physics, Vol. I*, pages 612–673, North Holland, The Netherlands, 1983.
60. M. Yan, L. C. Lee, and E. R. Priest. Fast magnetic reconnection with small shock angles. J. Geophys. Res., **97**, 8277 (1992).
61. V. N. Zharkov. *Estructura Interior de la Tierra y de los Planetas*. MIR, Moscow, 1985.